

Summer 2019

Endogenous Gene Tagging of pfr2 and pfr5 in *Trypanosoma cruzi* Using CRISPR/Cas9

Naomi Bryant

Central Washington University, bryantn@cwu.edu

Follow this and additional works at: <https://digitalcommons.cwu.edu/etd>



Part of the [Parasitology Commons](#)

Recommended Citation

Bryant, Naomi, "Endogenous Gene Tagging of pfr2 and pfr5 in *Trypanosoma cruzi* Using CRISPR/Cas9" (2019). *All Master's Theses*. 1248.

<https://digitalcommons.cwu.edu/etd/1248>

This Thesis is brought to you for free and open access by the Master's Theses at ScholarWorks@CWU. It has been accepted for inclusion in All Master's Theses by an authorized administrator of ScholarWorks@CWU. For more information, please contact scholarworks@cwu.edu.

ENDOGENOUS GENE TAGGING OF *PFR2* AND *PFR5* IN *TRYPANOSOMA CRUZI*
USING CRISPR/CAS9

A Thesis

Presented to

The Graduate Faculty

Central Washington University

In Partial Fulfillment

of the Requirements for the Degree

Master of Science

Biology

by

Naomi Nicole Bryant

August 2019

CENTRAL WASHINGTON UNIVERSITY

Graduate Studies

We hereby approve the thesis of

Naomi Nicole Bryant

Candidate for the degree of Master of Science

APPROVED FOR THE GRADUATE FACULTY

Dr. Gabrielle Stryker, Committee Chair

Dr. Lucinda Carnell

Dr. Blaise Dondji

Dean of Graduate Studies

ABSTRACT

ENDOGENOUS GENE TAGGING OF *PFR2* AND *PFR5* IN TRYPANOSOMA CRUZI USING CRISPR/CAS9

by

Naomi Nicole Bryant

August 2019

The flagellum of *Trypanosoma cruzi* contains the paraflagellar rod (PFR) an extra-axonemal scaffolding. The PFR consists of a lattice of cytoskeletal filaments that lies alongside the (9 + 2) microtubular axoneme, beginning at the flagellar pocket and extending to the flagellar tip. The PFR has only been observed within the phylums Euglenozoa and Dinoflagellata, although many eukaryotic organisms with long flagella have extra-axonemal structures that accommodate enzymes and regulatory proteins along with serving as scaffolding. The exact function and basic molecular composition of the PFR has yet to be determined although the major structural components, PFR1 and PFR2 and several minor proteins have been identified. The PFR is not only a complex structure that has been shown to be critical for motility, it also constitutes a unique set of proteins that are known to be immunogenic and provide protective immunity to *T. cruzi*. PFR5, a hypothetical minor component of the PFR, contains a PFR internal domain and an SH3 binding domain. Currently, it is unknown if the protein product of *pfr5* localizes to the flagellum. We have adapted a CRISPR/Cas9 endogenous gene tagging protocol to tag *pfr5* and investigate the subcellular localization of the protein. PFR2 localization serves as a proof of principle for this system as localization is well established. This technique allows for the precise insertion of a small 3x hemagglutinin tag at the C-terminus of the

gene of interest, with subsequent protein product also containing the tag. Localization of the tagged proteins is can then be visualized using immunofluorescence. Successful utilization of this technique, as well as localization of PFR5, will contribute to further the research and understanding of this unique structure.

ACKNOWLEDGMENTS

We would like to thank Roberto Docampo (pUC_sgRNA and Cas9/pTREX-n) and George Cross (pMOTag2H) for supplying the plasmids used in this study. We would also like to thank Gabrielle Stryker, Blaise Dondji, Lucinda Carnell, Noah Gorski, Drew Wilson, and the CWU biology department for their many contributions to this project. This project funded by the CWU school of graduate studies (Graduate Student Research Support Award and Graduate Student Summer Fellowship) the CWU Biology department (Washington Distinguished Fellowship in Biology), and the Stryker lab.

TABLE OF CONTENTS

Chapter		Page
I	INTRODUCTION	1
II	LITERATURE REVIEW	3
	Discovery of <i>T. cruzi</i>	3
	Morphology and Life Cycle	4
	Epidemiology	9
	Clinical Manifestation	10
	Immune Response and Evasion	12
	Paraflagellar Rod Immunogenicity	18
	CRISPR/Cas9 Discovery	22
	Adaptive Immunity in Prokaryotes	26
	Using CRISPR/Cas9 for Gene Editing in the Lab	29
III	MATERIALS AND METHODS.....	32
	Construct Preparation.....	32
	Cell Transfection.....	38
	PCR Confirmation.....	40
IV	RESULTS	41
	Selection of sgRNA Sequences.....	41
	sgRNA Amplification	42
	Subcloning sgRNA into Cas9/pTREX-n	45
	Donor DNA.....	54
	Transfections and Antibiotic Selection	56
	Transfection Confirmation	62
V	DISCUSSION.....	64
	LITERATURE CITED	70

LIST OF TABLES

Table	Page
1 Primers used in construct preparation and gene tagging confirmation. Underlined text for sgRNA primers indicates gene specific protospacer, while for donor DNA it indicates homologous arms. Bolded text indicates BamHI restriction sites	35
2 Set up of the six cuvettes used during a single round of transfection.....	39
3 CaCl ₂ protocols tested for transformation of <i>E. coli</i> with sgRNA/Cas9/pTREX-n ligation solutions	49
4 Electroporation protocols tested for transformation of <i>E. coli</i> with sgRNA/Cas9/pTREX-n ligation solutions.....	51
5 Set up of the four cuvettes used during the first transfection protocol tested.....	60
6 Set up of the four cuvettes used during the second transfection protocol tested.....	60
7 Set up of the three cuvettes used during the third transfection protocol tested.....	60

LIST OF FIGURES

Figure		Page
1	Illustration of the morphological forms of <i>T. cruzi</i> , including the location of the kinetoplast, nucleus, and flagellum (Modified from Wheeler, 2011).....	5
2	Illustration showing the location of the paraflagellar rod within the flagellum (Wheeler, 2006).....	7
3	Illustration detailing (1) the arrangement of the CRISPR locus and the transcription/translation of the components required for immunity (2) formation of individual crRNA:tracrRNA/Cas9 complexes from a single pre-crRNA transcript (3) final structure of the complex used to induce double stranded breaks within phage DNA (Modified from Hegasy).....	29
4	Maps of the plasmids used in the (A) amplification of sgRNA, (B) creation of sgRNA/Cas9 plasmid, and (C) the amplification of donor DNA. (A) The pUC_sgRNA plasmid contains the sequence for tracrRNA and an ampicillin resistance gene. (B) The Cas9/pTREX-n plasmid contains a ribosome promoter, HX1 trans-splicing site, GFP fused Cas9, and neomycin and ampicillin resistance genes. (C) The pMOTag2H plasmid contains a 3xhemagglutinin (HA) tag, tubulin intergenic region, and puromycin and ampicillin resistance genes. Maps made using benchling.com.....	37
5	Layout of the limiting dilution performed with epimastigotes transfected with <i>pfr2</i> specific constructs. Bolded well (A1) represent initial inoculum that was diluted 2-fold down the first column (green arrow) and then diluted 2-fold across (blue arrows) the 96 well plate.....	39
6	EuPaGDT results for selected guide sequences (A) <i>pfr2</i> and (B) <i>pfr5</i>	41

LIST OF FIGURES (CONTINUED)

Figure	Page
<p>7 Agarose gel electrophoresis images showing the results of the three different PCR reaction set ups tested for sgRNA amplification. (A and B) Results of the first two PCR set ups tested. These set ups were only used for <i>pfr2</i> sgRNA amplification and both resulted in the faint bands present within the red boxes. (C) Result of the final PCR set up tested. This agarose gel image is representative of what both <i>pfr2</i> and <i>pfr5</i> sgRNA amplification looked like. Expected size for all sgRNA amplification was 122bp.....</p>	44
<p>8 Representative agarose gel electrophoresis photo showing the digestion of sgRNA and Cas9 with BamHI-HF. Expected sizes: sgRNA (122bp) and Cas9 plasmid (11.2kB).</p>	48
<p>9 Agarose gel electrophoresis images showing the results of the PCRs done to confirm presence sgRNA/Cas9/pTREX-n plasmid in the bacterial colonies from the various transformation protocols tested. (A) Colony PCR of the colonies produced by the modified CaCl₂ and the electroporation protocol (Table 2, column 2; Table 3 column 1). (B) Representative image showing PCR of plasmid DNA from colonies produced by the further modified electroporation protocol (Table 3, column 3). (C) PCR of the plasmid DNA from the colony produced by the 2nd CaCl₂ protocol (Table 2, column 3). (D) Representative image showing the PCR of plasmid DNA from colonies produced by the CaCl₂ protocol described within the methods. Expected size was 190bp</p>	53
<p>10 Clustal omega DNA sequence alignments of sgRNA/Cas9/pTREX-n plasmids for (A) <i>pfr2</i> and (B) <i>pfr5</i>. Bolded sequences are BamHI restriction sites, underlined sequences are guide sequences, red sequences are tracrRNA, and asterix indicate matching nucleotide.....</p>	54
<p>11 Representative agarose gel electrophoresis images of donor DNA amplification for gene tagging of (A) <i>pfr2</i> and (B) <i>pfr5</i>. Expected sizes of 1.3kB (A) and 1.1kB (B).</p>	56
<p>12 Illustration detailing how all the transfections from table 7 were diluted and plated 24 hours post transfection.</p>	61

LIST OF FIGURES (CONTINUED)

Figure	Page
13 Representative agarose gel electrophoresis images showing the amplification of <i>pfr2</i> sgRNA from genomic DNA of parasites transfected with <i>pfr2</i> sgRNA/Cas9pTREX-n plasmid and donor DNA cassette. (A) From parasites transfected using the second transfection and antibiotic selection protocol. (B) From parasites transfected using the fourth transfection and antibiotic selection protocol. Expected size of 190bp.....	63

CHAPTER I

INTRODUCTION

Trypanosoma cruzi, the causative agent of Chagas disease, is currently estimated to infect 8 million people worldwide and cause 10,000 deaths per year (WHO, 2019-A). Treatments for Chagas disease are limited to benznidazole or nifurtimox, with varying efficacy rates due to stage of disease and drug resistance (Sales Junior et al., 2017). Due to these efficacy rates, the search for new drugs as well as vaccinations is heightened. Currently, there is no vaccination for Chagas, but several vaccine targets have been found over years of research. One such target is the paraflagellar rod (PFR), which is an extra-axonemal structure composed of cytoskeletal filaments that extends from the flagellar pocket to the tip of the flagellum (Portman and Gull, 2010). The proteins of PFR make good vaccine targets as they are highly conserved among strains of *T. cruzi*, are not homologous to human proteins, and are immunogenic (Clark et al., 2005). Immunization with purified PFR proteins as well as recombinant PFR has shown to provide immunity against *T. cruzi*, in mice (Wrightsmann et al., 1995).

The protein composition of the PFR is not fully known although research has revealed a core set of proteins that make up the PFR family (PFR1, PFR2, PAR1, and PAR4); all of these proteins, except PAR4, share a highly conserved 32aa region known as the PFR domain (Clark et al., 2005). Since the discovery of this family new proteins with a PFR domain have been discovered. PFR5 and PFR6 are among those discovered, with PFR5 having an additional SH3 binding domain, which has not been seen in any of the other PFR proteins (Clark et al., 2005). It has yet to be confirmed if these proteins do localize to the PFR.

The purpose of this study is to determine the localization of PFR5 utilizing a new technique, in *T. cruzi*, for protein localization. Currently, the most common methods for protein localization in *T. cruzi* are monoclonal antibodies and overexpression of tagged proteins. Both methods have been used to successfully locate proteins in *T. cruzi*, but they do have their drawbacks. Monoclonal antibodies can be cross reactive if the protein of interest is homologous in sequence to other proteins within the organism (Lander et al., 2016). Protein overexpression can in some cases lead to toxicity or inaccurate interpretation of results due to the high levels of protein produced and improper folding (Moriya, 2015). Due to these potential drawback's researchers have been pushing towards the use of CRISPR/Cas9 technology to tag genes endogenously.

Lander et al. (2016) developed one of the first protocols for C-terminal gene tagging in *T. cruzi* using CRISPR/Cas9. This protocol uses a gene specific sgRNA/Cas9 plasmid and donor DNA cassette to induce homology driven repair and insertion of a small 3x hemagglutinin tag (Lander et al., 2016). Subsequent protein product of the gene can then be localized using a hemagglutinin specific fluorescently conjugated antibody. In this study, we utilized this protocol to look at localization of PFR5 and PFR2, with PFR2 functioning as a proof of principle.

CHAPTER II
LITERATURE REVIEW

Discovery of *T. cruzi*

Trypanosoma cruzi was initially identified by Carlos Chagas in 1908 during an anti-malaria campaign for the Central do Brasil Railroad (Kropf and Sa, 2009). During the campaign Chagas set up a small laboratory in the rural settlement of Lassance. It was within Lassance that Chagas was made aware of a hematophagous insect that was known to frequently bite the faces of the local people (Kropf and Sa, 2009). Due to his previous knowledge of vector transmission, Chagas speculated that these insects may harbor a pathogen that could be transmitted to humans. Dissection of these insects revealed a flagellated protozoan, more specifically a trypanosome, within the hindgut (Kropf and Sa, 2009). In order to determine if this trypanosome could infect a mammalian host, Chagas sent several of the insects to his mentor Oswaldo Cruz, who exposed lab-bred marmosets to the insects (Kropf and Sa, 2009). Of those marmosets that became ill after exposure, Cruz found a form of the trypanosome within the blood (Kropf and Sa, 2009). Chagas soon after realized that this was a new species of trypanosome and named it *T. cruzi*, after his mentor Oswaldo Cruz (Kropf and Sa, 2009).

Suspecting that humans could be hosts to *T. cruzi*, Chagas began screening the people of Lassance for the parasite. On April 14, 1909, Chagas came across a feverish two-year-old girl with enlarged lymph nodes, liver, and spleen (Kropf and Sa, 2009). Subsequent testing of her blood revealed the presence of *T. cruzi*. Due to the presence of the parasite and the similarity of the child's symptoms to that of previous animal

research, Chagas concluded that this was the first case of a new disease, that would go on to be called Chagas disease (Kropf and Sa, 2009).

Although Chagas is the most prominent figure in regard to *T. cruzi*, he is not the only one to have contributed to its early identification and characterization, with some of the more notable contributors being Stanislaus Von Prowazek, Gaspar de Oliveira, and Alexandre Joseph Emile Brumpt (Steverding, 2014). Of the three individuals Prowazek, a Czechoslovakian zoologist and parasitologist, is the most acknowledged by Chagas himself, with Chagas publicly stating that his work on *T. cruzi*'s life cycle within the intermediate host was done under his guidance (Kropf and Sa, 2009). Vianna, a Brazilian pathologist, described the presence of the intracellular form (amastigote) of *T. cruzi* within skeletal and heart muscle cells (Steverding, 2014). Brumpt, a French pathologist, established that the mechanism of vector transmission was through getting insect feces in the bite wound rather than the bite itself (Steverding, 2014). Since the initial identification of *T. cruzi* in the early 1900s research has continued to expand on the ideas set forth by Chagas and fellow scientists.

Morphology and Life Cycle

Throughout its life cycle *T. cruzi* takes on several distinct morphological forms (amastigote, epimastigote, and trypomastigote) within the insect and mammalian host. These forms can be easily identified by the position of the kinetoplast (modified mitochondria which houses its own DNA known as kDNA) relative to where the flagellum emerges. Amastigotes are the smallest of the three forms (25µm X 2µm) and reside within the cytoplasm of mammalian host cells (de Lana et al., 2010). Their kinetoplast is situated in the center of the cellular body, anterior to the nucleus and

posterior to the base the short flagellum (figure 1). Amastigotes are the only form with a flagellum that does not extend out of the cellular body. Epimastigotes (20-40µm) are found within the intestine of the insect vector with their kinetoplast situated similarly to amastigotes, but unlike amastigotes, they have a flagellum that originates anteriorly of the nucleus and extends down past the cellular body (figure 1) (de Lana et al., 2010). Trypomastigotes (17µm) are the form infectious to both the insect vector and the mammalian host and reside in either the feces of the insect or the blood stream of the host (Martins et al., 2012). Their kinetoplast is situated at the most posterior end of the parasite, at the base of the flagellum. The flagellum originates posteriorly of the nucleus and extends anteriorly past the cellular body (figure 1).

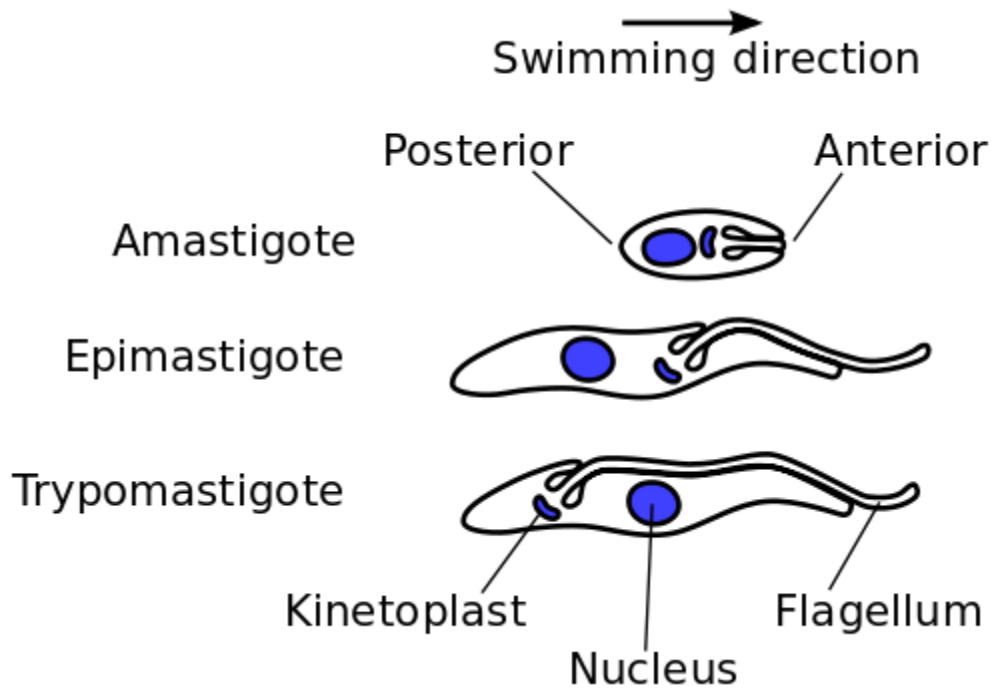


Figure 1 Illustration of the morphological forms of *T. cruzi*, including the location of the kinetoplast, nucleus, and flagellum (Modified from Wheeler, 2011).

The life cycle of *T. cruzi* begins with an infected Triatomine bug. These insects typically come out at night to take blood meals and are attracted to CO₂. Due to this attraction, they often bite near the face, thus earning their nickname the kissing bug. While taking a blood meal these insects will often defecate in order to make room for the incoming blood meal. Within the feces, is where the infectious form of the parasite, the metacyclic trypomastigote, resides. When the feces comes in contact with the bite wound or a mucosal membrane, typically through scratching the bite site, the trypomastigotes will enter the cells at the site of infection. Once inside the trypomastigotes will transform into amastigotes, as the trypomastigote form is the only form unable to go through replication. The amastigotes will then go through several rounds of replication via binary fission, before transforming back into trypomastigotes and rupturing from the cell. The newly released trypomastigotes will then go on to infect neighboring cells or travel through the bloodstream to other parts of the body. When a kissing bug takes a blood meal from an infected individual, they will take up trypomastigotes traveling through the bloodstream. Within the intestinal tract of the insect, the trypomastigotes transform into epimastigotes and replicate via binary fission. As the epimastigotes move towards the rectum, they transform into metacyclic trypomastigotes that are released with the feces.

In addition to its unique life cycle and morphological forms, *T. cruzi* also has several structures that differentiate it from other eukaryotes. One such structure is the paraflagellar rod (PFR). The PFR is a lattice structure of cytoskeletal filaments that lies along the (9+2) microtubular axoneme and extends from the flagellar pocket to the tip of the flagellum (figure 2) (Portman and Gull, 2010). The exact structural organization and protein makeup of the PFR is not fully understood although research has provided insight

on the general organization of the filaments as well as some of the major proteins. The filaments are arranged in a trilaminar manner with proximal, intermediate, and distal layers (Portman and Gull, 2010). The proximal and distal layers share similar overall structure with plates that contain thick (25nm) and thin (7nm) filaments that cross one another at 100° angles, the proximal layer contains two plates while the distal contains 11 (Farina et al., 1986). The intermediate layer is composed mainly of thin filaments which connect the proximal and distal layers (Farina et al., 1986). The PFR is attached to the microtubule axoneme through 4-7 electron dense filaments that connect the proximal domain to doublets 4 and 7 in the axoneme (Farina et al., 1986).

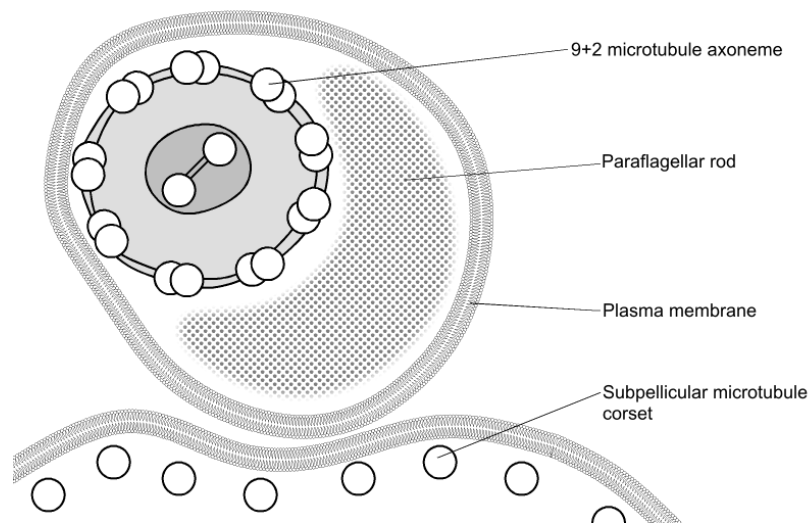


Figure 2 Illustration showing the location of the paraflagellar rod within the flagellum (Wheeler, 2006).

Along with the identification of the distinct layers, a core set of proteins (PFR1, PFR2, PAR1, and PAR4) belonging to the PFR family have also been identified. Most of the protein within this family share a highly conserved 32 amino acid region known as the PFR domain (Clark et al. 2005). Of the proteins within the family, PFR1 and PFR2 were the first two to be discovered. PFR1 and PFR2 were initially identified during a

study that compared purified flagellar proteins of an organism with a PFR (*Euglena gracilis*) to one without (*Chlamydomonas reinhardtii*) (Hyams, 1982). SDS-PAGE analysis of the purified proteins revealed two proteins, at 80 kDa (PFR1) and 69 kDa (PFR2), which were present within *E. gracilis* and not in *C. reinhardtii* (Hyams, 1982). Proof of these proteins' association with the PFR came in a later study that showed that PFR enriched flagellar preparations were predominantly composed of PFR1 and PFR2, due to the presence of the two bands seen during SDS-PAGE (Cunha et al., 1984). Subsequent research by Fouts et al. (1998) provided more insight into the proteins within these bands and revealed that each band actually contained two proteins instead of one; one band containing PFR1 and PAR1, and the other PFR2 and PAR4. Fouts et al. (1998) also provide proof of PFR localization for PAR1, PAR4, and PFR1 in *T. cruzi* using immunofluorescence. Since the initial discovery of the four core proteins two other proteins, PFR5 and PFR6, thought to belong to the PFR family have been discovered. In a study done by Clark et al. (2005), researchers searched sequence databases for sequences containing PFR domains. What the researchers found were two proteins, designated PFR5 and PFR6, with PFR5 found to have the additional motif of an SH3 binding domain (Clark et al., 2005). Since their initial discovery, it is unknown if these proteins localize to the PFR, as their family grouping would suggest, and if they do where within the PFR they are.

In regard to the function of the PFR, like the organization, it is not fully known but one function has become apparent over years of research. The PFR seems to function as support structure for the flagellum, aiding in motility. Several research studies have shown that removal of certain PFR proteins lead to decreased motility. One such study

done by Lander et al. (2015) found that CRISPR mediated knockout *pfr1* and *pfr2* in *T. cruzi* lead to improper formation of the PFR and detachment of the axoneme from the cell body. The consequence of this improper formation was paralysis of the organism, indicating PFRs strong role in motility.

Epidemiology

T. cruzi has three main cycles of transmission, sylvatic (wild), peridomestic, and domestic. In the sylvatic cycle, species of the Triatomine subfamily (mainly *Triatoma spp.*, *Rhodnius prolixus*, and *Panstronglus megistus*), transmit *T. cruzi* among over 100 mammalian species from eight orders (Marsupilia, Xenarthra, Rodentia, Primata, Carnivora, Chiroptera, and Artiodactyla) in the Americas and southern US (Jansen and Roque, 2010; Bern et al., 2011). Mammals are the only sylvatic host for *T. cruzi* as birds, reptiles, and amphibians are unable to maintain the life cycle due to complement factors in their blood that trypomastigotes are unable to combat (Jansen and Roque, 2010). Mechanisms of transmission in the sylvatic cycle include contamination of the bite wound with infectious feces following blood meal from triatomine, ingestion of infected triatomine (seen with the omnivorous mammals), and ingestion of prey infected with *T. cruzi* (seen with carnivores) (Jansen and Roque, 2010). Infection via fecal contamination follows the traditional life cycle of *T. cruzi* while ingestion changes the initial infection from one that originates at the skin to one that starts in the gastrointestinal tract.

The peridomestic and domestic cycles both involve domestic animals (cats, dogs, pigs, sheep, goats, etc.) but differ in how they are maintained (Bezerra et al., 2014). The peridomestic cycle originated from the sylvatic cycle but now involves the transmission of *T. cruzi* among domesticated animals in a fashion similar to the sylvatic (Coura and

Dias, 2009). The domestic cycle involves the transmission of *T. cruzi* between humans and domesticated animals through domesticated triatomine (Coura and Dias, 2009). These triatomine differ from the sylvatic in that they have become accustomed to living within and around human dwellings; *T. infestans*, *T. dimidiata*, and *R. prolixus* are the most often associated with the domestic cycle (Breniere et al., 2010). The types of dwellings associated with domestic triatomine are seen in poor or rural areas, and often have mud walls and thatched roofing. This type of housing provides triatomine with ample spots to hide in during the day. Domestic triatomines propensity to live in poor dwellings is the main driver behind the geographic distribution of Chagas disease and the number of cases seen. Chagas disease is predominately found in Latin America where the vector is found, with imported cases also showing up in the US, Canada, and Europe; the US has an estimate 300,000 individuals with Chagas (CDC, 2019-A). The main mode of transmission in endemic areas involves vector transmission, with the contamination of the bite wound or mucosal membrane with infectious feces. Other modes of transmission that account for a small portion of cases are congenital (from infected mother to newborn), blood transfusion, organ transplant, and contaminated food/beverage (usually contaminated with infectious triatomine feces) (CDC, 2019-A). Methods to curb the domestic cycle of *T. cruzi* have focused mainly on vector transmission and blood transfusions, with many endemic areas implementing vector control methods (pesticides and home improvements) and blood screening protocols (WHO, 2019-B)

Clinical Manifestation

Chagas disease presents itself in two main phases, acute and chronic. The acute phase begins shortly (1-2 weeks) after initial infection with *T. cruzi* and typically lasts 4-

8 weeks (Bern et al., 2011). During this time most infected individuals will either have mild symptoms, such as a fever and swollen lymph nodes or remain asymptomatic. In some cases, individuals can present with more prominent or severe symptoms. The symptoms can be a combination of fever, headache, fatigue, swelling at the site of infection (Romana's sign for the eyelid or chagoma for the skin), enlarged spleen/liver, swollen lymph nodes or cardiac/neurological alterations (Rassi et al., 2010). Death can occur in the acute phase but is uncommon and most often due to inflammation of the heart/brain (Rassi et al., 2010). Due to most infected individuals being asymptomatic or having non-specific symptoms many go undiagnosed. For those who have a clinical presentation (often Romana's or chagoma) or suspect they have been infected, blood smears and Polymerase chain reactions (PCR) tests can be used to confirm infection, due to the high levels of parasitemia seen during this phase (Bern et. al, 2011).

Treatment for acute Chagas comes in the form of two antitrypanosomal drugs, nifurtimox and benznidazole. Nifurtimox was the first drug ever used to treat Chagas and has a cure rate 88-100% for individuals who complete the full course of treatment during the acute phase (8-10mg/kg 4 times a day for 90 days) (Sales et al., 2017; CDC, 2019-B). Side effects most commonly associated with nifurtimox include nausea, vomiting, weight loss, tingling of the extremities, and drowsiness (Sales et al., 2017). Currently, nifurtimox is not the recommended course of treatment and is no longer used in endemic areas, due to its tendency to produce more severe side effects than its counterpart (Sales et al., 2017). Benznidazole, the preferred drug, has a cure rate of around 80% following completion of the treatment in the acute phase (5-8mg/kg twice a day for 60 days) (Sales et al., 2017; CDC, 2019-B). The most common side effects are tingling of the extremities,

nerve pain, and weight loss (Sales et al., 2017). Due to the symptoms, both treatments can cause many individuals to either have gaps in their treatment or not finish.

For those who do not receive or finish treatment during the acute phase, they will enter the indeterminate chronic phase. This phase begins two to three months after initial infection and is characterized by continuous low levels of circulating parasite (Rassi et al., 2010). Individuals within this phase are asymptomatic and can remain so for the rest of their life. In some cases, indeterminate individuals will enter the chronic phase, which occurs 20-30 years after initial infection and is characterized by two complications. 20-30% of indeterminate individuals will go on to develop cardiac complications such as heart failure, irregular heartbeats, or the formation of blood clots (WHO, 2019-B; Rassi et al., 2010). 10% of individuals will go on to develop digestive complications which can manifest in dilatation of the colon or esophagus, termed megacolon or megaesophagus (WHO, 2019-B). Diagnosis of chronic Chagas cannot be made using blood smears, like in acute, since parasite levels are low, instead serological techniques like ELISA, or PCR tests are used (Bern et al., 2010). Treatment of chronic Chagas is more about symptom management as the drugs available in the acute phase are not curative for the chronic phase. Although not curative benznidazole has been shown to slow the progression of cardiac complications in some chronic individuals (Sales et al., 2017).

Immune Response and Evasion

Host Cell Entry

Following entry through the bite wound or mucosal membrane, metacyclic trypomastigotes will enter either the cells of the tissue (ex. fibroblasts) or innate immune system (ex. macrophage) (Truyens and Carlier, 2010). Cells of the tissue are

preferentially infected at the start of infection due to the parasites limited ability to migrate to draining lymph nodes and its desire to stave off recognition by the immune system (Padilla et al., 2009). Entry into non-phagocytic cells follows one of two routes: lysosome dependent or invagination of the cell membrane with subsequent lysosomal fusion (Cardoso et al. 2015). Regardless of which pathway is chosen, host cell entry begins with the binding of *T. cruzi* glycosylphosphatidylinositol (GPI) surface proteins to their receptor on the host cell (de Pablos and Osuna, 2012; Bartholomeu et al., 2014). Binding of GPI initiates the PI3K pathway, which results in the release of Ca^{2+} in the host cell (Rodriguez et al., 1995). The lysosome dependent route utilizes this increase Ca^{2+} to drive lysosomes to the cell membrane (Rodriguez et al., 1996). Fusion of the lysosomes with the cell membrane allows the parasite to enter the cell through an acidic parasitophorous vacuole (vacuole containing a parasite). The invagination route utilizes the PI3K pathway by entering the cell membrane in a region that is rich with phosphatidylinositol trisphosphate (PIP_3), resulting in the formation of a parasitophorous vacuole (Woolsey et al., 2003). The vacuole goes on to fuse with early endosomes and then lysosomes, resulting in the same acidic vacuole as the lysosome dependent route (Woolsey et al., 2003).

The acidification of the parasitophorous vacuole does not harm the trypomastigote rather it aids in its transition to amastigote and exit from the vacuole. The internal membrane of the vacuole is composed mainly to two sialylated proteins, lysosome-associated membrane proteins (LAMP) 1 and 2, which help to prevent destruction of the vacuole (Kornfeld and Mellman, 1989; Hall et al., 1992; Alberetti et al., 2010). *T. cruzi*, on its surface, has *trans*-sialidase which in conditions of low pH will release from

parasite and become active (Cardoso et al., 2015). The active *trans*-sialidase remove sialic acid from LAMP 1 and 2 and transfer them to the surface on the parasite (Albertti et al., 2010; Hall et al., 1992). The removal of sialic acid causes the vacuole to become susceptible to pore-forming proteins which cause the vacuole to lyse, allowing amastigotes to enter the cytosol and begin replication (Andrews et al., 1990).

Innate Immune Response

Macrophages present in the tissue at the time of infection are the first immune cells to come in contact with *T. cruzi*. In order to recognize *T. cruzi* and initiate an immune response, macrophages have membrane bound receptors known as toll like receptors (TLRs), on the surface of the cell and within endosomes (Acevedo et al., 2018). These TLRs detect pathogens through the recognition of pathogen associate molecular patterns (PAMPs). When *T. cruzi* encounters the surface of a macrophage they activate TLR2/6 and 4; TLR2/6 recognize GPI while TLR4 recognizes glycoinositolphospholipids (GIPLs) (Junquera et al., 2010; Oliveira et al., 2004; Campos et al., 2001). When *T. cruzi* enters macrophages through phagocytosis, they activate TLR7 and 9 within the parasitophorous vacuole, which recognize parasite RNA and DNA respectively (Bafica et al., 2006; Caetano et al., 2011). Activation of a TLR initiates the Myd88 pathway, in the case of TLR2/6, 4, 7, and 9, and the TRIF pathway in the case of TLR4 (Truyens and Carlier, 2010; Rodrigues et al., 2012). The Myd88 pathway leads to the production of the pro-inflammatory cytokines TNF α (only produced by TLR2/6 activation) and IL-12, while the TRIF pathway produces the type-1 interferons INF α/β (Trinchieri and Sher, 2007; Rodrigues et al., 2012). Production of these cytokines and interferons initiate the innate immune response to *T. cruzi*,

specifically: TNF α permeabilizes the blood vessels allowing immune cells to enter the site of infection, IL-12 brings natural killer (NK) cells to the site of infection and activates them, and INF α/β increases expression of NK receptor ligands while also activating NK cells. Activated NK cells will release IFN γ , activating macrophages and increasing their propensity for phagocytosis. Production of pro-inflammatory cytokines also induces the production of nitric oxide within the parasitophorous vacuole (Munoz-Fernandez et al., 1992). Nitric oxide (NO) functions to kill *T. cruzi* by inhibiting vital cysteine rich proteins, like cruzipain, or producing peroxynitrite which decreases membrane integrity and induces apoptosis by impairing mitochondrial function (Radi, 2013; Venturini et al., 2000; Alvarez et al., 2011). To combat oxides produced by macrophages *T. cruzi* has peroxidases that detoxify the vacuole (Piacenza et al., 2008).

T. cruzi, specifically trypomastigotes, are exposed to another aspect of the innate immune system after they rupture from a host cell and travel to the bloodstream. Within the bloodstream, there are proteins for three complement pathways (alternative, lectin, and classical) which all work to tag pathogens for opsonization, recruit immune cells, and perforate cell membranes. Each pathway is activated in a different manner before converging in the formation of C3 convertase. The alternative pathway is activated when C3 is spontaneously cleaved into C3b and attached to the surface of the parasite. Binding of C3b initiates the formation of C3 convertase. The lectin pathway is activated by the binding of mannose-binding lectin and ficolins to *N*-glycans (Cestari et al., 2009). This complex cleaves C4 and C2 to form the C3 convertase. The classical pathway is activated by the binding of *T. cruzi* specific antibodies and C1. C1 cleaves both C4 and C2 to form C3 convertase. In order to combat either the activation of a pathway or the formation of

C3 convertase *T. cruzi* has several molecules on its surface, calreticulin (TcCRT), *T. cruzi* complement C2 receptor inhibitor trispanning (TcCRIT), *T. cruzi* complement regulatory protein (TcCRP), and trypomastigote decay acceleration factor (T-DAF). TcCRT inhibits activation of the lectin and classical pathway by inhibiting the function of mannose-binding lectin and C1 (Ferreira et al., 2004; Sosoniuk et al., 2014). TcCRIT functions by inhibiting the formation of C3 convertase, in the classical pathway, through competing with C4 in binding to C2 (Cestari et al., 2008, 2009). TcCRP inhibits the formation of C3 convertase in all three pathways by binding either C3b or C4b (Lidani et al., 2017; Norris et al., 1991). Lastly, T-DAF interferes with the overall formation of the C3 convertase in the alternative, classical, and possibly the lectin pathways (Joiner et al., 1988; Tambourgi et al., 1993).

Adaptive Immune Response

The move from innate to adaptive immunity comes with the migration of dendritic cells from infected tissue to the lymph nodes. Within the tissue dendritic cells function similarly to macrophages in that they readily phagocytose parasites, which activate TLRs and lead to production of pro-inflammatory cytokines. Where dendritic cells differ from macrophage is in the purpose for up taking parasites. Instead of trying to clear the immediate infection, dendritic cells prioritize processing *T. cruzi* antigen so that it can be presented on the cell surface via major histocompatibility complexes (MHC) class I and II to cell of adaptive immunity. MHCs class I is present on most cells within the body while MHC class II is present only on professional antigen presenting cells including dendritic cells, B cells, macrophage, and T cells. During their migration to the lymph nodes, dendritic cells undergo a maturation process where they increase

expression of MHC class II, costimulatory molecules (CD40, CD80, and CD86) that aid in T cell activation, and pro-inflammatory cytokines (Van Overtvelt et al., 1999). *T. cruzi* can inhibit this process by downregulating IL-12, TNF α , CD40 and MHC class II, thus delaying the start of adaptive immunity (Overtvelt et al., 1999).

Once mature dendritic cells reach the lymph nodes CD8 T cells are first activated through binding of MHC class I on dendritic cells (Truyens and Carlier, 2010). Following activation, CD8 T cells leave the lymph node and search for cells infected with *T. cruzi*. Identification of infected cells is done through the binding of the T cell receptor to an MHC class I complex that contains antigen for *T. cruzi*. Successful binding results in release of cytotoxic granules which kill the infected cells as well as the release IFN γ to increase antigen presentation and macrophage activation. Back in the lymph node, dendritic cells are also activating CD4 T cells through MHC class II. Activated CD4 T cells can either help in the activation of CD8 T cells through binding of MHC class II on CD8 T cells or leave the lymph node in search for infected macrophage. Once infected macrophage are located through binding of MHC class II, CD4 T cells release IFN γ to activate macrophage and induce killing of the parasites within the parasitophorous vacuoles. Returning to the lymph node again B cells with *T. cruzi* specific antibody are also being activated with the help of T follicular helper (T_{FH}) cells. Activation occurs through the binding of MHC class II on the B cells and release of cytokines by the T_{FH}, which cause the B cells to differentiate into a plasma cell and begin releasing antibodies. The goal of these antibodies is to tag extracellular *T. cruzi* for opsonization.

Collectively all of the mechanisms used to target *T. cruzi* during the adaptive immune response do little to fully clear the infection. This is due to the mechanisms *T.*

T. cruzi has developed to diminish the effectiveness of effector cells. One method by which *T. cruzi* does is through the presentation of highly variable antigens, which increases the time it takes to find an antigen that works to effectively target *T. cruzi*. (Truyens and Carlier, 2010). This results in the production of polyclonal antibodies and T cells that are essentially non-functional in this system. In addition, some of these antigens do not stimulate a strong proliferative response in T or B cells thus limiting the population of effector cells (Truyens and Carlier, 2010). Another way in which *T. cruzi* limits the population of effector cells is through the release of active *trans*-sialidase. These active sialidase can bind mucin on the surface of lymphocytes and induce apoptosis, decreasing cell populations (Mucci et al., 2002). Lymphocyte apoptosis can also result from the high levels of NO and TNF α produced during the immune response to *T. cruzi* (Truyens and Carlier, 2010). The cell debris created also aids in the suppression of the immune response through the production of TGF β , which suppresses macrophage activation and T cell function, following phagocytosis (Truyens and Carlier, 2010).

Paraflagellar Rod Immunogenicity

PFR's immunogenic properties were initially identified in a study that immunized mice with cell fractions from epimastigotes and then challenged them with a lethal dose of trypomastigotes (Segura et al., 1976). Of the cell fractions used the flagellar fraction was the most effective, with 90% of the mice surviving compared to the 0-50% seen with the other fractions (Segura et al., 1976). This study showed the ability of the flagellum to be protective in an acute infection scenario, but not in a chronic. Building on these results another study immunized mice with similar cell fractions but challenged with a lower dose of trypomastigotes (Ruiz et al., 1985). What they found, like the previous study, was

that the flagellar fraction was the most effective. Mice that were immunized with the purified flagellar fraction had fewer instances of positive xenodiagnoses (feeding blood to the insect vector and the checking the vector for parasites) and showed no signs of heart inflammation (potential complication of chronic Chagas disease) (Ruiz et al., 1985).

Following the positive results seen with the flagellar fraction, researchers investigated the proteins of the flagellum to find possible antigens that could be used in a vaccine. The proteins of the PFR became of interest due to the PFR being a unique structure found only in the Euglenids and Kinetoplasts. The first study to look at the PFR as a source of antigen, isolated PAR1 and PFR2 for immunization of mice with subsequent lethal challenge (Wrightsmann et al., 1995). What this study found was that mice immunized subcutaneously survived (100%) lethal challenge, while mice immunized intraperitoneally did not (Wrightsmann et al., 1995). In addition, both vaccination methods produced antibodies specific PAR1 and PFR2, with intraperitoneal producing significantly more (Wrightsmann et al., 1995). The significant difference in survival post challenge provided the first hint that immunity towards *T. cruzi* may not be mediated by antibodies. Instead, one study by Miller et al. (1997) concluded that immunity following immunization with PFR was mediated by CD4 and CD8 T cells, and did not require antibodies. This conclusion was founded, in part, by immunizing mice either genetically deficient in B cells or MHC class 1, or depleted of CD4 T cells and challenging them with a lethal dose of *T. cruzi* trypomastigotes (Miller et al., 1997). The results of the B cell and MHC class 1 experiments were reported as parasitemia and number of survivors, with the B cell deficient mice having reduced parasitemia and 100% survival, and the MHC class 1 deficient mice having increased parasitemia and 0%

survival 20 days post challenge (Miller et al. 1997). Both of these results enforce the conclusion that T cells rather than B cells are required for *T. cruzi* immunity. The results of the CD4 T cell depleted mice were more focused on parasitemia post challenge, as all of the PFR immunized mice survived, unlike the MHC class 1 deficient mice (Miller et al., 1997). The parasitemia of the immunized mice remained at constant high for 80 days post challenge, only decreasing once CD4 T cell populations were allowed to regrow (Miller et al., 1997). These results show that CD4 and CD8 T cells are required for complete immunity with CD8 T cells being critical for survival and CD4 T cells being critical for parasite clearance. In addition to looking at the overall importance of immune cells, macrophage activation by IFN γ production was explored through *in vitro* experiments using T cells from immunized mice and the immunization and subsequent challenge of mice genetically deficient in IFN γ (Miller et al., 1997). The results of the *in vitro* experiments showed that CD4 T cells from immunized mice produced high levels of IFN γ in comparison to CD8 and naïve T cells (Miller et al., 1997). The results of the *in vivo* study showed that mice deficient in IFN γ were unable to survive past 19 days post infection due to increased levels of parasitemia, which were higher than those seen in the other genetically deficient mice (Miller et al., 1997). Both the *in vitro* and *in vivo* studies indicate the importance of CD4 T cells and their production of IFN- γ in *T. cruzi* immunity and clearance.

The mechanism by which PFR primed CD4 and CD8 T cells are able to recognize infected cells starts with *T. cruzi* entering the vacuole of a cell and beginning its transition from trypomastigote to amastigote. During this transition, the parasite will duplicate its kinetoplast and flagellum before going through cytokinesis (Kurup and Tarelton, 2014).

This results in one daughter cell having a nucleus, kinetoplast, and shortened flagellum (characteristic of amastigotes), while the other has no nucleus, a kinetoplast, and the longer original flagellum (Kurup and Tarelton, 2014). The reason for this uneven division is thought to be the result of the long flagellum being too difficult for the parasite to absorb or dissolve, so it disposes of it (Kurup and Tarelton, 2014). Following the division, the vacuole dissolves and the daughter cells are released into the cytoplasm (Kurup and Tarelton, 2014). The amastigote goes on to replicate while the other daughter cell is transported to the proteasome where it is degraded (Kurup and Tarelton, 2014). The degraded remnants are then either transported to the endoplasmic reticulum, where they are loaded into MHC class 1 or they are transported to vesicles containing MHC class 2.

This mechanism of disposing of the flagellum allows for the proteins of the PFR to be some of the first *T. cruzi* antigens presented to CD4 and CD8 T cells (Kurup and Tarelton, 2014). Activated CD4 T cells release IFN- γ , which activates macrophages by increasing phagocytosis and production of nitric oxide (Miller et al., 1997). Activated CD8 T cells can also release IFN- γ , although at a lower rate than CD4 T cells, in addition to the release of granzymes which initiate death of an infected host cell (Kurup and Tarelton, 2014). Priming of the immune system with PFR protein either purified or recombinant allows for the development of a pool of PFR specific CD4 and CD8 T cells that can swiftly recognize *T. cruzi* infected cells shortly after infection. Thus, allowing for the immunity seen in immunization studies.

CRISPR/Cas9 Discovery

The first description of clustered regularly interspaced short palindromic repeats (CRISPR) was by Ishino et al in 1987. At the time Ishino was working on a project where he was sequencing a 1.7Kb region of the *Escherichia coli* genome that contained the isozyme of alkaline phosphatase (*iap*) gene (Ishino et al., 1987). It was while analyzing the sequence downstream of the *iap* gene that Ishino et al. (1987) found five homologous sequences (29nt long) that were spaced 32nt apart. In addition to this unusual clustering, the group found that the center of the homologous regions contained palindromic sequences (Ishino et al., 1987). At the time the research group did not understand the function of these repeated sequences but did acknowledge the unique finding in their publication on *iap*. Soon after this discovery, other research groups found similar repeats in *Shigella* spp. and *Mycobacterium tuberculosis*, indicating that *E. coli* was not unique (Nakata et al., 1989).

Several years after the initial discovery in *E. coli*, similar repeats were found within the archaea *Haloflex mediterranei* (1993) and *H. volcanii* (1995) (Mojica et al.). This discovery was unique, as these repeats had previously only been found in bacteria. In an attempt to elucidate the role of these repeats in *Haloflex* spp. the researchers behind these discoveries, Mojica et al. (1995), transformed the archaea with recombinant plasmids containing these repeats. What they found was that the addition of extra repeats decreased cell viability as well as lead to differing DNA distribution among dividing cells (Mojica et. al; 1995). Due to these results, the researchers proposed that the repeats function in the partitioning of replicated DNA into daughter cells (Mojica et. al; 1995). Mojica went on to test this partitioning hypothesis in *E. coli* but did not find the same

results, suggesting a different function for these repeats (Monjica et al., 2016).

The late 90s saw a revolution in DNA sequencing, with new techniques allowing for the publication of the first complete genome sequence of a free-living organism (*Haemophilus influenzae*) (Fleischmann et al., 1995). Following this publication, the number of complete genomic sequences for bacteria and archaea increased, with a total of 26 publicly available by the end of the 90s (Monjica et al., 2016). While sequencing these genomes, researchers began to find repeats similar to those found by Ishino and Mojica, but since there were no programs available to accurately identify these repeats, they could often be difficult to find. In a study done by Mojica et al. (2000), they were able to utilize a computer program to search complete and partial genomes for these repeats, at the time called Short Regularly Spaced Repeats (SRSRs). The results of these searches showed that SRSRs were only present in bacteria and archaea and were not confined to particular phylogenetic groups. In addition, Mojica et al (2000). provided a concise description of the main features of SRSRs: (1) short sequences (24-40bp) with an up to 11bp long palindromic region (2) repeated sequences are arranged in clusters, with up to 14 clusters in one genome (3) unique spacer sequences (20-58bp) separate the repeats within a cluster (Mojica et al., 2000). This set of features indicated that SRSRs serve a common function among the bacteria and archaea that have them.

The influx of complete and partial genomic sequences not only help Mojica begin to elucidate the true function of SRSRs but also aided in the discovery of several genes associated with them. In a study by Jansen et al. (2002) they used a computer program, similar to Mojica et al., to expand on the list of organisms with SRSRs (renamed to the universally accepted CRISPR). While searching for CRISPR loci the researchers also

looked at common genes that flanked the loci. What they found were four genes, designated CRISPR-associated genes (cas) 1-4, that were present in prokaryotes with loci and absent in those without the loci (Jansen et al., 2002). Not all CRISPR containing prokaryotes had all of the cas genes but they did have cas1 in conjunction with one or more of the three other genes (Jansen et al., 2002). The researchers were not able to determine how CRISPR loci and cas genes interacted but were able to predict, based on structure, that the proteins for cas3 and cas4 were most likely involved in DNA modification and DNA binding respectively (Jansen et al., 2002).

Shortly after the discovery of the cas genes two independent labs, Mojica et al. (2005) and Pourcel et al. (2005), published similar findings on the spacer regions within the CRISPR loci. Both labs sequenced the loci of various prokaryotes and compared them to known sequences in the GeneBank database. What they found was that many of the spacer sequences were homologous to regions within bacteriophage genomes (Mojica et al. and Pourcel et al., 2005). To hypothesize the purpose of these homologs, both groups turned to previous publications that focused on whole genome sequencing. The product of these literature searches revealed that prokaryotes containing spacers for a particular bacteriophage did not contain any DNA from that phage within its genome (Mojica et al. and Pourcel et al., 2005). Since genome integration is vital for the bacteriophage lysogenic lifecycle it was concluded that the CRISPR loci could be conferring immunity against particular phages. In addition to these common findings, both groups provided separate conclusions on the mechanism behind immunity or how new spacers may be incorporated. Mojica et al. (2005) found during their sequencing efforts that the spacers often targeted genes necessary for phage survival and replication. The targeting of these

genes in conjunction with prior knowledge that CRISPR loci produce RNA transcripts lead them to the conclusion that immunity could function similar to eukaryotic RNAi (Mojica et al., 2005). Pourcel et al. (2005) found when comparing the order of spacers between the loci of their related prokaryotes that newer spacers were added to the front of the loci. This led them to suggest that insertion of new spacers is most likely done by simultaneously duplicating the homologous region at the beginning of the loci and inserting the spacer.

Building on the idea that CRISPR functioned similar to RNAi Makarova et al. (2006) performed an analysis of Cas protein sequences to determine their functions and find functional analogies to proteins within the RNAi system. What they found were analogous proteins for dicer, slicer, and RNA-dependent RNA polymerase (Makarova et al., 2006). In addition, they proposed that the spacer regions performed similar functions to siRNAs by binding to specific sequences, such as invading DNA and targeting them for degradation (Makarova et al., 2006). Within their conclusion, Makarova et al. (2006) pointed out that although CRISPR had many analogies to RNAi this system also resembled adaptive immunity within vertebrates, due to its memory component. CRISPR's role in bacterial adaptive immunity was experimentally shown in 2007 by (1) infecting *Streptococcus thermophilus* with bacteriophage and examining their CRISPR loci (2) removing spacers from *S. thermophilus* and testing their susceptibility to phage infection (Barrangou et al.). The results of the first set of experiments showed that post infection, those bacteria that developed resistance had acquired new spacer sequences at the proximal end of the CRISPR locus (Barrangou et al., 2007). In addition, factors such as which spacers were acquired, number of spacers acquired, and the presence/absence of

single nucleotide polymorphisms affected phage immunity (Barrangou et al., 2007). The results of the second set of experiments revealed that removal of particular spacers decreased immunity to particular phages (Barrangou et al., 2007). Since the publishing of the study, much of the process by which the various components of CRISPR function to produce adaptive immunity has been pieced together.

Adaptive Immunity in Prokaryotes

Adaptive immunity in prokaryotes follows three main steps: (1) adaptation – acquisition of new spacer sequences from invading bacteriophage, (2) crRNA biogenesis – transcription and processing of the CRISPR array, and (3) targeting – crRNA guided Cas endonucleases cleaves invading DNA (Barrangou and Marraffini, 2014). The proteins and protein complexes utilized in each step can vary among prokaryotes with the CRISPR-Cas system diverging into six main types. These six types (I, II, III, IV, V, VI) differ mainly in the type of endonuclease used to cleave foreign DNA, with type I using Cas3, type II Cas9, type III Cas10, type IV Csf1, type V Cpf1, and type VI Cas13 (Makarova et al., 2015). Type II (Cas9) is the most commonly used type in gene editing research due to its use of only a single multidomain nuclease to induce double stranded breaks within the DNA.

Using the type II system as an example for adaptive immunity in prokaryotes, the process of adaptation starts with the transcription of *cas1* and *cas2* (proteins part of the *cas* operon). Cas1 and Cas2 form a complex responsible for cleaving portions (25-65nt) of invading DNA and inserting them at the proximal end of the CRISPR array (region of the CRISPR locus that contains all of the spacers and repeats; serves as the memory bank for the immune system) (Mir et al., 2018). In some cases, *csn2* is present in the *cas*

operon and is transcribed along with *cas1* and *cas2* (Mir et al., 2018). The exact function of Csn2 in spacer acquisition is not fully understood but it has been noted that it is able to bind to the Cas1/Cas2 complex (Ka et al., 2018). This ability to bind has hinted at the possibility of Csn2 serving as a scaffold that helps to anchor the proteins of the Cas1/Cas2 complex together (Ka et al., 2018).

Following reinfection with a bacteriophage that has been logged into the CRISPR array, crRNA biogenesis occurs. In this biogenesis, the CRISPR array, *cas9*, and tracrRNA (sequence that contains a homologous region to the repeats within the array) are all transcribed (figure 3). The CRISPR array is often transcribed as a single transcript called pre-crRNA that is then further processed to produce individual crRNA (Hille and Charpentier, 2016). There are some instances where there are promoters within the repeated sequences, allowing for varying length of pre-crRNA (Hille and Charpentier, 2016). Following transcription of the array, tracrRNA binds to its complementary sequence in the repeat creating an RNA duplex that can be bound by Cas9 (figure 3) (Hille and Charpentier, 2016). Following the formation of the duplex, RNase III separates the individual pre-crRNA:tracrRNA complexes from one another, producing mature crRNA (figure 3) (Hille and Charpentier, 2016).

The mature crRNA is used in the targeting step, to guide Cas9 endonucleases to invading DNA. This guiding is accomplished by the spacer region in the mature crRNA binding to its complementary sequence with the bacteriophage DNA. Once bound to this sequence Cas9 will cleave the DNA, rendering it incapable of continuing infection; crRNA's often target regions important for phage survival, such as DNA replication and phage integration (Mojica et al., 2005). Within the Cas9 endonuclease, there are two

domains (HNH and RuvC) which administer cuts to the invading DNA (Doudna and Charpentier, 2014). HNH induces a break within the strand complementary to the crRNA, while RuvC induces a break in the other strand (Doudna and Charpentier, 2014). The presence of both domains within one nuclease is what has made the Cas9 system the preferred system for gene editing.

The binding crRNA to its complementary sequence is not the only thing required for Cas9 to cut. Small sequences known as protospacer adjacent motifs (PAM) must be present either directly upstream or downstream of the target site. The purpose of the PAM sequence is to make the CRISPR/Cas system specific for foreign DNA and prevent self-targeting (Hille and Charpentier, 2016). Due to this PAM requirement, Cas9 is sometimes used to select spacers before Cas1, Cas2, and Csn2 incorporate them into the CRISPR array (Mir et al., 2018). Following the recognition of a PAM site by Cas9's PAM interacting domain (PID), Cas9 will induce its double stranded break 3nt upstream of the PAM sequence, effectively inhibiting infection (Mir et al., 2018).

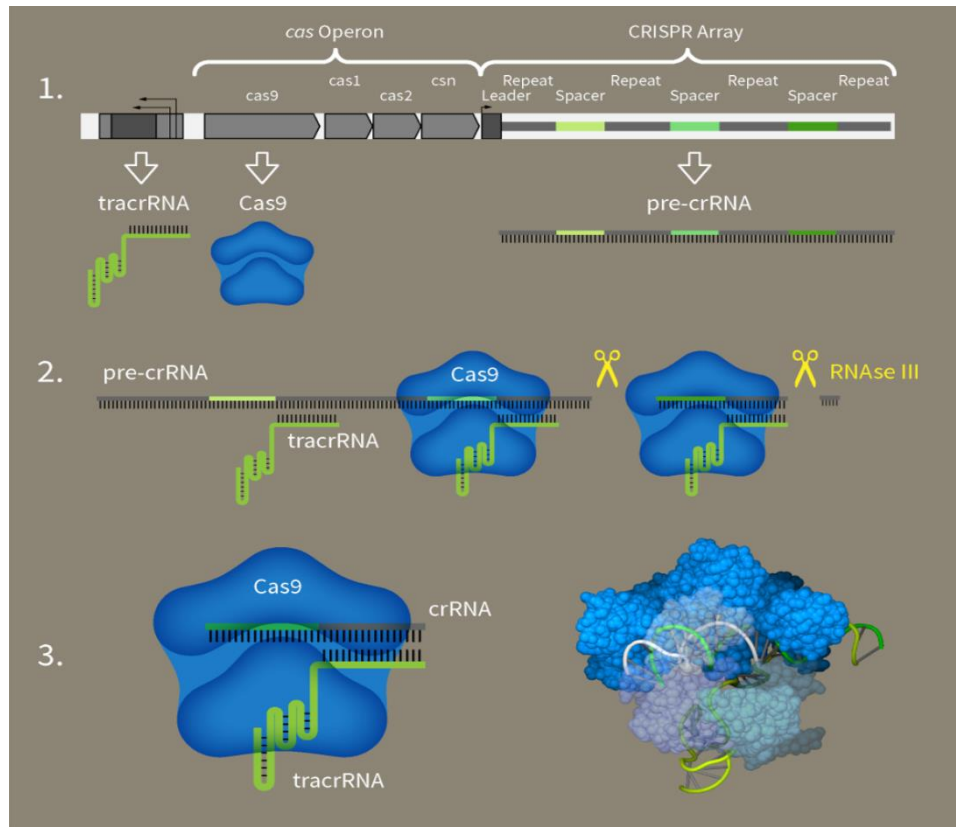


Figure 3 Illustration detailing (1) the arrangement of the CRISPR locus and the transcription/translation of the components required for immunity (2) formation of individual crRNA:tracrRNA/Cas9 complexes from a single pre-crRNA transcript (3) final structure of the complex used to induce double stranded breaks within phage DNA (Modified from Hegasy).

Using CRISPR/Cas9 for Gene Editing in the Lab

CRISPR/Cas9 within a laboratory setting has been modified from its prokaryotic origins to utilize, in its most basic format, a Cas9 endonuclease and a single guide RNA (sgRNA). The sgRNA combines a unique spacer region, selected by the researcher, and tracrRNA that can be expressed within a single transcript. These two components can take on a variety of forms when being transfected or injected into organism, such as: 2 separate plasmids (one for sgRNA and one for Cas9), a single plasmid (with both sgRNA and Cas9), rna transcripts of both components, or a rna transcript of the sgRNA and protein complex of Cas9 (Thurtle-Schmidt and Lo, 2018). Regardless of the format used

the end result is a Cas9/sgRNA complex that is able to deliver a double stranded break at a specific location within the genome.

Using the single plasmid method as an example, as it is one of the more common methods used, CRISPR/Cas9 gene editing starts with selecting a region within a genome to edit and selecting a spacer sequence. The spacer sequence is around 20nt long and contains the point at which the gene editing event, a double stranded break, will occur. When selecting a spacer sequence, the location of PAM sequences (5'- NGG -3' for *Streptococcus pyogenes*, the most commonly used endonuclease) has to be taken into consideration since Cas9 cannot function without its presence (Addgene, 2017). The requirement of this PAM sequence is one of the limitations of this technology, as if one is not available near the desired target region then another method of gene editing may have to be used. Another point that must be taken into consideration when selecting a spacer sequence is the likelihood of off target cuts with a particular sequence. The likelihood of this kind of event depends on the degree of similarity between a chosen spacer sequence and other sequences within a genome. To minimize the chance of choosing a sequence with high likelihood, many researchers utilize computer programs whose sole purpose is to provide spacer sequence options.

Following selection of the sequence, the spacer must be incorporated into the sgRNA structure. This can be accomplished by designing DNA oligos that contain the spacer sequence and using them to amplify a plasmid that contains the sequence for the tracrRNA, resulting in copies of a single sequence that contains both the spacer and the tracrRNA sequence. Once amplified, the sgRNA can be cloned into a plasmid that contains the sequence for the Cas9 endonuclease. This single plasmid contains both

sgRNA and Cas9, which can then be transfected or injected into the desired organism. Within the organism, the contents of the plasmid will be expressed and processed, producing Cas9 endonucleases that are guided by sgRNA. These guided Cas9's will induce double stranded breaks 3nt upstream of the PAM sequence (Mir et al., 2018). This double stranded break can be repaired by either non-homologous end joining (NHEJ) or homology directed repair (HDR). Non-homologous end joining is the more common mechanism for repair as it does not require template DNA for repair, rather it relies on ligation of the two ends of the break. Due to the lack of a template this mechanism can lead to insertions or deletions of nucleotides, resulting in mutations (Addgene, 2017). The potential for mutations allows this mechanism of repair to be exploited for CRISPR/Cas9 gene knockouts. Homology directed repair, the less efficient of the two repair mechanisms, utilizes template DNA that is homologous in sequence to the region that requires repair. In the case of gene editing via CRISPR/Cas9 the template DNA comes in the form of donor DNA that is transfected/injected along with the sgRNA/Cas plasmid. The donor DNA contains a desired insert, which is flanked by two regions of homology (homologous arms) that correspond to either side of the break. The use of donor DNA allows researchers to insert various sequences, such as mutations, gene tags, or antibiotic resistance genes into specific regions within the genome.

CHAPTER III

MATERIALS AND METHODS

Trypanosoma cruzi Culture

CL Brenner strain epimastigotes were cultured in Schneider's complete media supplemented with 20% heat-inactivated fetal calf serum (FCS) (Gemini, Lot# A77F00H). Transformants were maintained in medium containing 100 µg/ml G418 and 5 µg/ml puromycin (sigma-aldrich, cat# P8833-10MG).

Construct Preparation

sgRNA Amplification

C-terminal tagging was performed according to Lander et al. (2016), utilizing both a sgRNA/Cas9 vector and a linear donor DNA cassette to facilitate homologous recombination. Protospacer sequences targeting the 3' end of *pfr2* and *pfr5* were designed using the Eukaryotic Pathogen CRISPR guide RNA Design Tool (EuPatGDT). PCR amplifications of sgRNA were performed using 40ng pUC_sgRNA plasmid gifted by Roberto Docampo (Addgene #68710) (Lander et al., 2015) (figure 4A), 0.4µM protospacer specific forward primer (Table 1, primers 1-2), 0.4µM sgRNA backbone reverse primer (Table 1, primer 3), 25µl Q5 high-fidelity 2x master mix (NEB, cat# M0492S), and nanopure H₂O (table 2) in a 50µl reaction. PCR conditions were: initial denaturation at 98°C for 2 min followed by 34 cycles of 98°C for 10s, 55°C for 20s, and 72°C for 20s, followed by a final extension at 72°C for 2 min. PCR product was isolated using the Zymo gel DNA recovery kit (Genesee scientific, cat# 11-300).

sgRNA Subcloning

sgRNA PCR product was subcloned into the Cas9/pTREX-n plasmid gifted by Roberto Docampo (Addgene #68708) (Lander et al., 2015) (figure 4B) using BamHI restriction sites and T4 DNA ligase (NEB, cat# M0202S). Digest conditions for both sgRNA and Cas9/pTREX-n plasmid were: 1µg sgRNA or plasmid, 1µl BamHI-HF (NEB, cat #R3136S), 5µl 10x cutsmart buffer (NEB, cat# B7204S), and nanopure H₂O, followed by a 1hr incubation at 37°C. Immediately following digestion, plasmid DNA was dephosphorylated by adding 1µl of calf intestinal alkaline phosphatase (CIAP) (Promega, cat# M1821) to the digested plasmid and incubating at 37°C for 30min. Digested sgRNA and plasmid were isolated using the Zymo gel DNA recovery kit. Ligation conditions for sgRNA and plasmid were: 50ng of digested plasmid, 37.5ng of digested sgRNA, 1µl T4 DNA ligase, 2µl T4 DNA ligase reaction buffer (NEB, cat# B0202S), and nanopure H₂O, followed by an overnight incubation in the refrigerator and ligase inactivation at 64°C for 10min.

Transformation

The ligation mixture was used to transform HB101 *Escherichia coli* as follows; 3ml of Luria-Bertani (LB) broth was inoculated with a single HB101 colony. This inoculated broth was then incubated overnight in a shaking incubator set at 37°C and 250rpm. 500µl of the overnight culture was then used to inoculate 50ml of LB broth. The newly inoculated broth was incubated for 3 hours in a shaking incubator set at 37°C and 150rpm, before incubating on ice for 30min. After incubation on ice, the entire volume of the culture was transferred to a 50ml conical tube and centrifuged at 6000rpm for 5min at 4°C. The supernatant was then poured off and the cell pellet was resuspended in 5ml of

50mM CaCl₂ and left to incubate for 20min on ice. Following incubation, the cells were centrifuged at 6000 rpm for 5min at 4°C. The supernatant was again poured off and the cell pellet was resuspended in 2.5ml of 50mM CaCl₂ with 10% glycerol. The cell suspension was then aliquoted into 0.7ml microcentrifuge tubes, 100µl per tube, and snap frozen using liquid nitrogen. When it came time to perform the transformation the desired number of aliquots were thawed on ice. After thawing 2µl of ligation mixture was added to the aliquots and they were incubated on ice for 30 min. The aliquots were then heat shocked cells at 42°C for 1 min before returning to ice. The heat shocked cells were then transferred to glass culture tubes with 1ml of LB broth and incubated for 2 hours in a shaking incubator set at 37°C and 250rpm. 1ml of the cultures was transferred and spread onto LB/ampicillin agar plates, which were incubated overnight at 37°C.

Colonies were checked for presence of sgRNA/Cas9/pTREX-n plasmid, with sgRNA in correct orientation, using PCR of plasmid isolated with the Zyppy plasmid miniprep kit (Genesee Scientific, cat# 11-308). 25µl reactions were performed using 20ng of plasmid DNA, 12.5ul Apex Taq RED Master Mix (Genesee Scientific; cat# 42-138), 0.4µM protospacer specific forward primer (Table 1, primers 1-2), 0.4µM of a reverse primer that binds to the HX1 trans-splicing site (Table, 1 primer 4), and nanopure H₂O. PCR conditions were: initial denaturation at 95°C for 3 min followed by 34 cycles of 95°C for 30s, 60°C for 20s, 72°C for 20s, followed by a final extension at 72°C for 5 min. Plasmid from positive PCR's were sequenced to confirm correction orientation and sequence of sgRNA. Prior to transformation multiple minipreps were performed and the plasmid DNA was pooled, and ethanol precipitated.

Donor DNA Amplification

Homologous arms for the Donor DNA cassettes were generated using 30nt (*pfr5*) or 100nt (*pfr2*) regions upstream and downstream of the estimated cut site (3nt upstream of the protospacer adjacent motif). Amplification of donor DNA cassettes was done using 50µl PCR reactions containing 40ng pMOTag2H plasmid gifted by George Cross (Addgene #26296) (figure 4C), 2µl DMSO, 25µl Q5 high-fidelity 2x master mix, 0.4µM forward and reverse primers containing homologous arms (Table 1, primer 5-8), and nanopure H₂O. PCR conditions were: initial denaturation at 98°C for 2/3 min (*pfr2/pfr5*) followed by 40/34 cycles (*pfr2/pfr5*) of 98°C for 20sec, 63/72°C (*pfr2/pfr5*) for 20s, and 72°C for 1min 40s/1 min (*pfr2/pfr5*), followed by a final extension at 72°C for 10/2 min (*pfr2/pfr5*). PCR product was purified using the DNA clean and concentrator kit (Genesee Scientific, cat#11-302C). Prior to transformation multiple PCRs were performed and the donor DNA was pooled, and ethanol precipitated.

Table 1 Primers used in construct preparation and gene tagging confirmation. Underlined text for sgRNA primers indicates gene specific protospacer, while for donor DNA it indicates homologous arms. Bolded text indicates BamHI restriction sites.

#	Primer name	5'-3' Primer sequence
1	PFR2-sgrna	GATCG GATC <u>CCTGGGTGGCACCGGCGGACACGTTTTAG</u> AGCTAGAAATAGC
2	PFR5-sgrna	GATCG GATCC <u>GACTAAAGAGCCTCCTCGTGGTTTTAG</u> AGCTAGAAATAGC
3	sgRNA-rv	CAGT GGATCC AAAAAAGCACCGACTCGGTG
4	HX1-rv	TAATTTCGCTTTCGTGCGTG
5	PFR2-HR1	<u>GGAGGAGGTGAAGATTGCGGCGGAGCGCGAGGAACTG</u> <u>AAGCGCTCCAAGACACTGCAGAGCCAGCAGTACCGCG</u> <u>GCAAGACGGTGCAGCAGATCACACAGGGTACCGGGCC</u> CCCCCTCGAG

6	PFR2-HR2	<u>CGGCAGTGGACTTGGTTTCCTATTTTTTCCTACAATGGA</u> <u>GATATTACATAAAAAACATACATGGAATGGGGAAAAC</u> <u>AGCAACAGCGTTGGGTGGCACCGGTGGCGGCCGCTCT</u> AGAACTAGTGGAT
7	PFR5-HR1	<u>ACAGGGCTATTTCCCATCAACTACGTTGTGGGTACCGG</u> GCCCCCCTCGAG
8	PFR5-HR2	<u>AAAAAAAAAAAAAAGAGTTTGTCTCACACACTGGCGGC</u> <u>CGCTCTAGAACTAGTGGAT</u>
9	Puro-rv	TCAGGCACCGGGCTTGCGGG
10	PFR2-fv	GGCATTGAGTTTGTGCATCCC

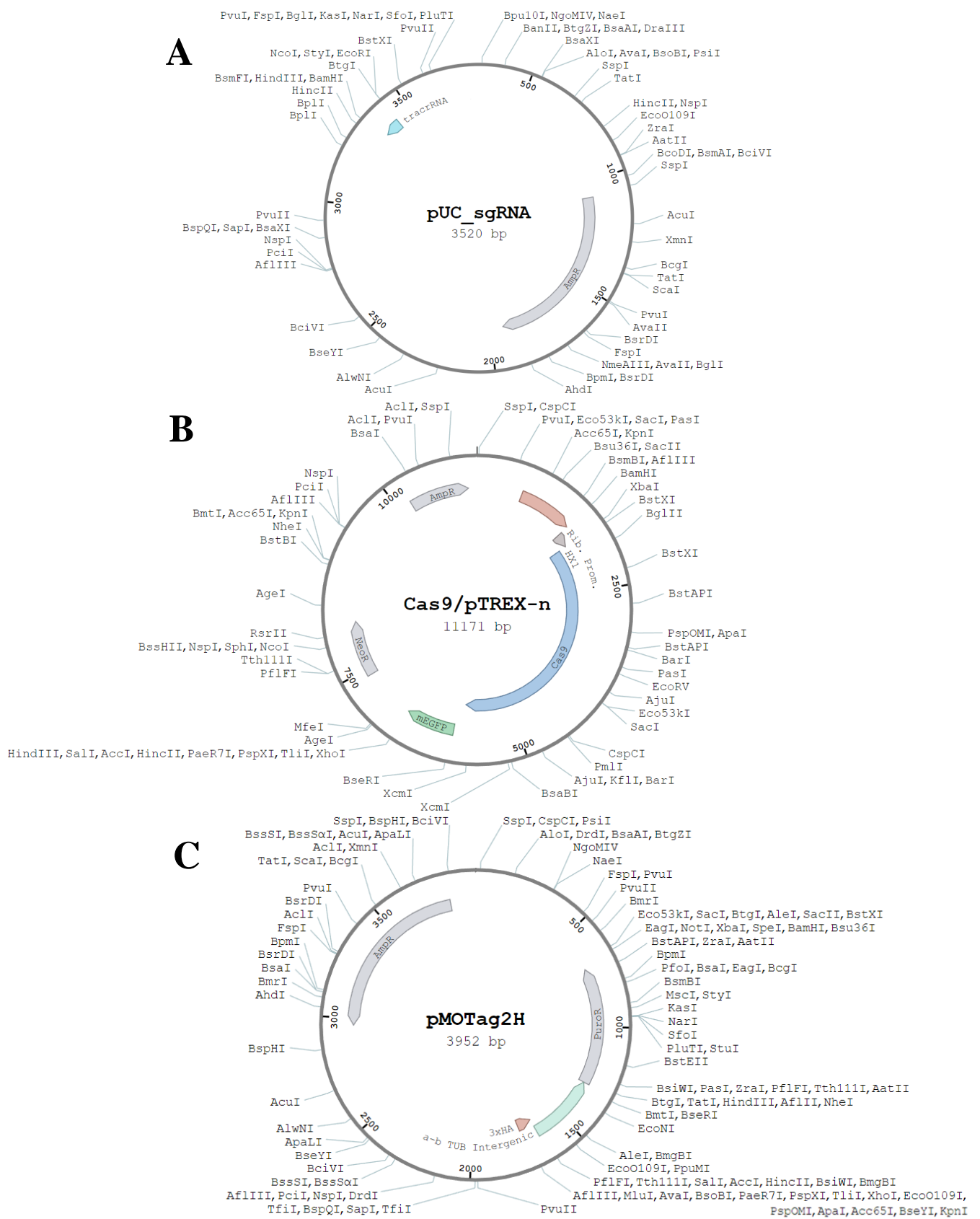


Figure 4 Maps of the plasmids used in the (A) amplification of sgRNA, (B) creation of sgRNA/Cas9 plasmid, and (C) the amplification of donor DNA. (A) The pUC_sgRNA plasmid contains the sequence for tracrRNA and an ampicillin resistance gene. (B) The Cas9/pTREX-n plasmid contains a ribosome promoter, HX1 trans-splicing site, GFP fused Cas9, and neomycin and ampicillin resistance genes. (C) The pMOTag2H plasmid contains a 3xhemagglutinin (HA) tag, tubulin intergenic region, and puromycin and ampicillin resistance genes. Maps made using benchling.com.

Cell Transfection

T. cruzi epimastigotes were cultured in Schneider's complete media supplemented with 20% FCS until reaching a density of $1-2 \times 10^7$ cells/ml. Once reaching this density cells were transferred to a 15ml conical tube and centrifuged at 1,200rpm for 10 min. The supernatant was then poured off and the cells were washed with 5ml of phosphate buffered saline (PBS) by resuspending the cell pellet in the PBS and then centrifuging at 1,200rpm for 10min. The supernatant was again poured off and the cell pellet was resuspended in cold Tb-BSF (5mM KCl, 0.15mM CaCl₂, 90mM Na₂HPO₄, 50mM HEPES, pH 7.3) at a concentration of 1×10^8 cells/ml. Following the layout presented in table 2, 400µl of epimastigotes, 10-25µg plasmid construct, and 10-25µg donor DNA was added to pre-chilled 2mm electroporation cuvettes (BTX, cat#45-0125). Before electroporation cuvettes were placed on ice for 10min. The BTX ECM 830 electroporation system was used to deliver 3 pulses (~1.3kV 100µs) to all cuvettes, with cuvettes being placed on ice for 1 min between each pulse. Following electroporation, epimastigotes were allowed to recover at room temperature for 15 min before being transferred to suspension culture flasks (Genesee scientific, cat# 25-213) containing 5ml of Schneider's complete media supplemented with 20% FCS. 24 hours after electroporation antibiotics (100 µg/ml G418 and 5 µg/ml puromycin) were added to the medium. The medium was changed each week by transferring the contents of the flasks to 15ml conical tubes, centrifuging at 800-1,200rpm for 10 min, pouring off the supernatant, and resuspending the cell pellet in 5ml of media with antibiotics. After 5 weeks under antibiotic selection epimastigotes transfected with *pfr2* specific plasmid and donor, DNA were diluted into 96 well plates (figure 5).

Table 2 Set up of the six cuvettes used during a single round of transfection.

Control	<i>Pfr2</i> transfection	<i>Pfr2</i> transfection	<i>Pfr5</i> transfection	<i>Pfr5</i> transfection	<i>Pfr5</i> sgRNA/Cas9 plasmid control
400µl 1x10 ⁸ cells/ml epimastigotes	31µl donor dna (24.7µg)	25µl donor dna (19.9µg)	35µl donor dna (24.7µg)	16µl donor dna (11.2µg)	4.8µl plasmid dna (3.8µg)
	28µl plasmid dna (24.9µg)	24µl plasmid dna (24.5µg)	31µl plasmid dna (24.7µg)	16µl plasmid dna (12.7µg)	80µl 1x10 ⁸ cells/ml epimastigotes
	400µl 1x10 ⁸ cells/ml epimastigotes	400µl 1x10 ⁸ cells/ml epimastigotes	400µl 1x10 ⁸ cells/ml epimastigotes	400µl 1x10 ⁸ cells/ml epimastigotes	



Figure 5 Layout of the limiting dilution performed with epimastigotes transfected with *pfr2* specific constructs. Bolded well (A1) represent initial inoculum that was diluted 2-fold down the first column (green arrow) and then diluted 2-fold across (blue arrows) the 96 well plate.

PCR Confirmation

Pfr2 sgRNA/Cas9/pTREX-n plasmid and donor DNA integration was assessed using PCR of genomic DNA from suspected double resistant mutants. Genomic DNA was obtained by centrifuging parasites at 1,200rpm for 10 min followed by resuspension in 50µl of nanopure H₂O and incubation at 60°C for 10 min. 25µl PCR reactions were performed using 5µl genomic DNA, 12.5µl Apex Taq RED Master Mix, 6.5µl nanopure H₂O, and 0.4µm forward and reverse primer (Table 1, Primers 1 and 4 for plasmid identification; primers 9 and 10 for donor DNA identification). PCR conditions for plasmid confirmation were: initial denaturation at 95°C for 3min, followed by 34 cycles of 95°C for 30s, 60°C for 20s, 72°C for 20s, followed by a final extension at 72°C for 5min. PCR conditions for gene tagging confirmation were: initial denaturation at 95°C for 3min, followed by 34 cycles of 95°C for 30s, 55°C for 30s, 72°C for 1min 40s, followed by a final extension at 72°C for 10min.

CHAPTER IV

RESULTS

Selection of sgRNA Sequences

Construction of gene specific sgRNA/Cas9/pTREX-n plasmids started with the selection of 20nt long guide sequences between 20nt upstream and 50nt downstream of the stop codon. Guide sequence selection was done using EuPaGDT, which is an online program that designs guide sequences by searching uploaded genomes for 20nt sequences next to protospacer adjacent motifs (PAM) (5'-NGG-3') (figure 6). In addition to finding guide sequences, EuPaGDT provides the number of off target hits for each designed guide sequence (figure 6). Following selection, guide sequences were incorporated into forward primers that contained a BamHI restriction site at the 5' end (Table 1, primers 1 and 2).

A

gRNA id (Gene_start-of-gRNA)	gRNA_sequence	gRNA match start	gRNA match end	alignment (top: gRNA, bottom: genomic match)	is on-target	alignment identity	genome annotation	match chromosome	chromosome match start	chromosome match end
1_506_revcom	TGGGTGACACCGCGGACAC AGG									
		1	23	TGGGTGACACCGCGGACACAGG TGGGTGACACCGCGGACACAGG	is on-target	100.00	No Annotation found. Possibly belongs to inter-genic region(s) or is an unannotated gene/gene-family-member	TcChr25-S	147827	147849

gRNA id (Gene_start-of-gRNA)	gRNA sequence	gRNA match start	gRNA match end	alignment (top: gRNA, bottom: genomic match)	matched PAM	alignment identity	genome annotation	match chromosome	chromosome match start	chromosome match end
1_506_revcom	TGGGTGACACCGCGGACAC AGG									
		no off-target hits								

B

gRNA id (Gene_start-of-gRNA)	gRNA_sequence	gRNA match start	gRNA match end	alignment (top: gRNA, bottom: genomic match)	is on-target	alignment identity	genome annotation	match chromosome	chromosome match start	chromosome match end
1_608_revcom	GACTAAAGAGCCTCCTCGTG CGG									
		1	23	GACTAAAGAGCCTCCTCGTGCGG GACTAAAGAGCCTCCTCGTGCGG	is on-target	100.00	TcCLB.509099.30: paraflagellar rod protein 5%2C putative	TcChr23-S	361716	361738

gRNA id (Gene_start-of-gRNA)	gRNA sequence	gRNA match start	gRNA match end	alignment (top: gRNA, bottom: genomic match)	matched PAM	alignment identity	genome annotation	match chromosome	chromosome match start	chromosome match end
1_608_revcom	GACTAAAGAGCCTCCTCGTG CGG									
		no off-target hits								

Figure 6 EuPaGDT results for selected guide sequences (A) *pfr2* and (B) *pfr5*.

sgRNA Amplification

The forward primers, containing the guide sequences, were used in conjunction with a reverse primer that also contained a BamHI restriction site, to amplify pUC_sgRNA plasmid that contained the sequence for tracrRNA (Table 1, primers 1, 2, and 3). Finding the correct PCR conditions for maximum amplification took several iterations before arriving at the reaction mixture and thermocycler program presented in the methods section. The first iteration included a 50µl PCR reaction with 40ng pUC_sgRNA, 25µl Q5 high-fidelity 2x master mix, nanopure H₂O, and 0.5µM sgRNA forward and reverse primers (Table 1, primers 1 and 3). The PCR conditions were: initial denaturation at 94°C for 2 min, followed by 34 cycles of 94°C for 15s, 52°C for 20s, and 72°C for 20s, followed by a final extension at 72°C for 20s. This set up was only used for *pfr2* sgRNA amplification and resulted in a faint band that appeared to be at the correct size (122bp) (figure 7A). For the next iteration, we increased the denature temperature, from 94°C to 98°C to align with the PCR protocol provided by the supplier of the polymerase. In addition, we decreased the concentration of primer used to one consistent with the standard PCR reaction set up utilized in our lab. This 25µl PCR reaction consisted of 40ng pUC_sgRNA plasmid, 12.5µl Q5 high-fidelity 2x master mix, nanopure H₂O, and 0.4µM sgRNA forward and reverse primer (Table 1, primers 1 and 3). The PCR conditions were: initial denaturation at 98°C for 3min, followed by 34 cycles of 98°C for 10s, 52°C for 20s, and 72°C for 20s, followed by a final extension at 72°C for 2 min. This set up was also only used for *pfr2* sgRNA amplification and resulted in a faint band that appeared to be at the right size (122bp) (figure 7B). For the final iteration, which is described in the methods, we increased the annealing temperature from 52°C to

55°C, which was a temperature calculated by the T_m calculator available by the supplier of the polymerase. This set up resulted in the brightest bands, at 122bp, and was used for the amplification of all the *pfr2* and *pfr5* sgRNA that was used in subsequent cloning (figure 7C). Prior to cloning all sgRNA PCR product was run on an agarose gel to confirm size; bands were excised from the gel and DNA was recovered using the Zymo gel DNA recovery kit.

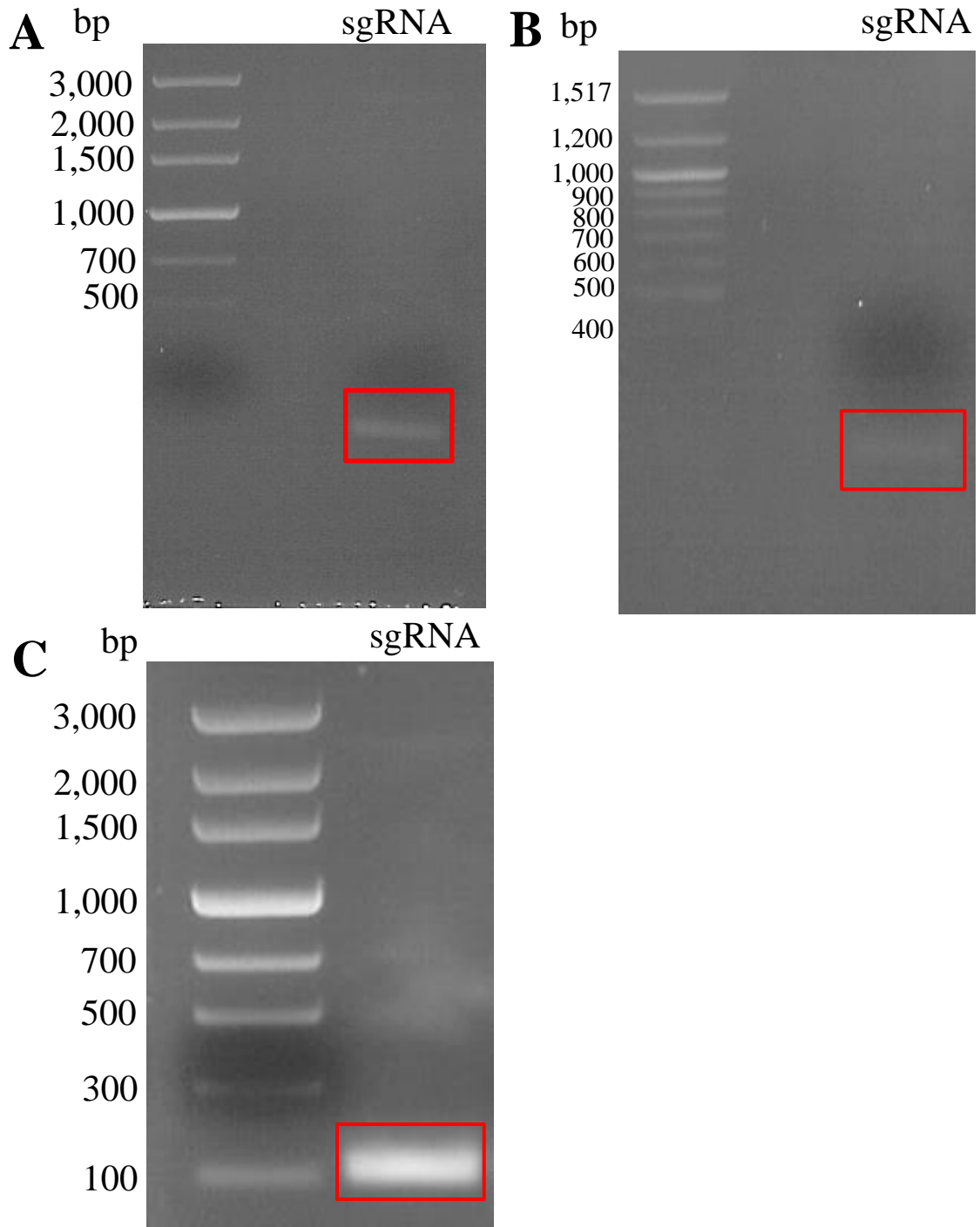


Figure 7 Agarose gel electrophoresis images showing the results of the three different PCR reaction set ups tested for sgRNA amplification. (A and B) Results of the first two PCR set ups tested. These set ups were only used for *pfr2* sgRNA amplification and both resulted in the faint bands present within the red boxes. (C) Result of the final PCR set up tested. This agarose gel image is representative of what both *pfr2* and *pfr5* sgRNA amplification looked like. Expected size for all sgRNA amplification was 122bp.

Subcloning sgRNA into Cas9/pTREX-n

Amplified and recovered sgRNA, for both *pfr2* and *pfr5*, was subcloned into Cas9/pTREX-n plasmid, between the ribosome promoter and HX1 trans-splicing site, using BamHI restriction sites on both the sgRNA and the plasmid. Prior to ligation, digestion of both was confirmed using agarose gel electrophoresis with product at the correct size (122bp sgRNA, 11.2kB Cas9/pTREX-n) being excised and recovered with the Zymo gel DNA recovery kit (figure 8). Following ligation, *E. coli* was transformed with the ligation mixtures. Several transformation protocols were tested before reaching the final version presented in the methods. The first protocol used was a CaCl₂ transformation using JM109 *E. coli* (Table 3, column 1). This method was used only with *pfr2*sgRNA/Cas9/pTREX-n ligation solution and resulted in no colony growth. For the next transformation the CaCl₂ protocol was modified by decreasing the amount of ligation solution added (5µl to 2µl), decreasing the length of the heat shock (2 min to 45s), and increasing the volume of cell transferred to the LB/AMP plates (100µl to 1ml) (Table 3, column 2). The reasons for these changes were to decrease the potential for the components of the T4 ligation reaction buffer to hinder transformation, decrease the potential for cell death during heat shock, and increase the likelihood of having at least one colony grow on the plates. This modified protocol resulted in the growth of several colonies, although the colonies were smaller than expected. At the same time, we performed this modified protocol, we also tried an electroporation protocol using JM109 *E. coli* (Table 4, column 1). This protocol also resulted in growth of several small colonies. In order to determine if these colonies contained *pfr2*sgRNA/Cas9/pTREX-n plasmid with the sgRNA in the correct orientation, we performed colony PCR on several

of the colonies from the CaCl₂ protocol and the electroporation protocol. The 25µl PCR reactions performed contained 12.5µl Q5 high-fidelity 2x master mix, nanopure H₂O, 5µl template DNA (one bacterial colony added to 5µl nanopure H₂O), and 0.8µM forward and reverse primer (Table 1, primers 1 and 4). The PCR conditions were: initial denaturation at 98°C for 2 min followed by 34 cycles of 98°C for 20s, 60°C for 20s, and 72°C for 20s, followed by a final extension of 72°C for 5 min. The results of the colony PCR showed the presence of bands below the expected size of 190bp, indicating the absence of the correct plasmid (figure 9A). For the next transformation we modified the electroporation protocol by using HB101 *E. coli* instead of JM109, changing the percentage of glycerol used (50% to 10%), increasing the amount of ligation solution used (1µl to 2µl), trying an additional electroporator setting (1,800v and 5ms), culturing the cells post electroporation, and transferring a larger volume of cell suspension to the LB/AMP plates (40µl to 100µl) (Table 4, column 2). The changes in glycerol percentage and electroporator settings were inspired by an undergraduate researcher (Noah Gorski) who was working on a protocol for bacterial electroporation. The change in *E. coli* strain was done to see if one strain was better at taking up the plasmid than the other, while the rest of the changes were done to increase likelihood of getting transformants on the plates. This protocol did not result in the growth of colonies. The next transformation was a modification of the previous modification, for the electroporation protocol. This modification increased the volume of ligation solution used (2µl to 5µl) replaced the 1,800v/5ms electroporator setting with the 2,500v/90µs setting and increased the culture time post electroporation (30 min to 1 hour). The protocol resulted in the growth of several colonies that also had satellite colonies. Due to the presence of these few colonies

this protocol was also used for the first time with *pfr5*sgRNA/Cas9/pTREX-n ligation mixture, which did not result in colony growth. The colonies from the *pfr2* electroporation were test for the presence of the plasmid using PCR of plasmid DNA isolated through the Zyppy plasmid miniprep kit. The 25µl PCR reaction included 1µl of plasmid DNA, 12.5µl of Apex Taq Red master mix, nanopure H₂O, and 0.4µM forward and reverse primer (Table 1, primers 1 and 4). The PCR conditions were initial denaturation at 95°C for 3 min, followed by 34 cycles of 95°C for 30s, 60°C for 20s, and 72°C for 20s, followed by a final extension at 72°C for 5 min. The results of this PCR showed the presence of several bands above the desired 190bp, indicating these bacteria did not contain the correct plasmid (figure 9B). The next transformation protocol tested was another CaCl₂ protocol, but with HB101 (Table 3, column 3). This protocol was used for both *pfr2*sgRNA/Cas9/pTREX-n and *pfr5*sgRNA/Cas9/pTREX-n ligation mixtures and resulted in the growth of a single colony on the *pfr5* transformed plate. This colony was tested for the presence of the plasmid in the same way the prior *pfr2*sgRNA/Cas9/pTREX-n electroporation colonies were tested (figure 9C). The results of the PCR were similar to that of the prior *pfr2* PCR, indicating that this bacterial colony did not contain the correct plasmid. The final transformation protocol tested was the one presented in the methods. This method used both the *pfr2*sgRNA/Cas9/pTREX-n and *pfr5*sgRNA/Cas9/pTREX-n ligation mixture and produced the most colonies and unlike the first couple of CaCl₂ transformations tried, this protocol produced bacterial colonies of an average size. Following the PCR protocol outlined in the methods, the colonies were tested for the presence of the plasmid, with sgRNA in the correct orientation. The results of the PCR showed the presence of a band at the 190bp for several of the colonies

tested (figure 9D). Plasmids that had a positive PCR amplification were sent to GenScript for Sanger sequencing. Results of the sequencing were checked against the expected sequence using the Clustal Omega sequence alignment tool (figure 10).

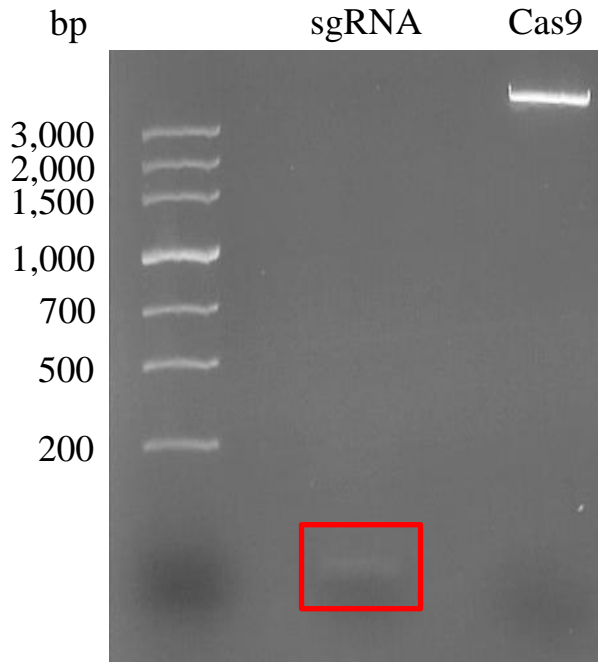


Figure 8 Representative agarose gel electrophoresis photo showing the digestion of sgRNA and Cas9 with BamHI-HF. Expected sizes: sgRNA (122bp) and Cas9 plasmid (11.2kb)

Table 3 CaCl₂ protocols tested for transformation of *E. coli* with sgRNA/Cas9/pTREX-n ligation solutions.

CaCl₂ transformation protocol (First protocol tested for <i>pfr2sgRNA/Cas9/pTREX-n</i> plasmid transformation)	Modification to CaCl₂ transformation protocol (Second protocol tested for <i>pfr2sgRNA/Cas9/pTREX-n</i> plasmid transformation)	CaCl₂ transformation protocol (Sixth protocol used for <i>pfr2sgRNA/Cas9/pTREX-n</i> plasmid transformation and second protocol used for <i>pfr5sgRNA/Cas9/pTREX-n</i> plasmid transformation)
1. Inoculated 3ml of LB broth with a single colony of JM109	12. Added 2µl of ligation mixture to cell suspension and heat shocked at 37°C for 45s	1. Inoculated 3 ml of LB broth with a single HB101 colony
2. Incubated inoculated culture overnight in a shaking incubator set at 37°C and 250rpm	14. Transferred and spread 1ml of the cell solution onto LB/AMP agar plates	2. Incubated inoculated broth overnight in shaking incubator set at 37°C and 250rpm
3. Inoculated 25ml of LB broth with 100µl of overnight culture		3. Transferred 100µl of overnight culture to 25ml LB broth and incubated for 3 hours in a shaking incubator set at 37°C and 150rpm
4. Incubated culture for 3 hours in a shaking incubator set at 37°C and 150rpm		4. Transferred culture to pre-chilled 50ml conical tube and centrifuged at 8,000 rpm for 5 min at 4°C
5. Incubated culture on ice for 30 min		5. Poured off supernatant and resuspended cell pellet in 5ml of cold 30mM CaCl ₂
6. Transferred chilled culture to a pre-chilled 50ml conical tube and centrifuged at 5,000rpm for 10min at 4°C		6. Distributed the cell suspension among 1.5ml microcentrifuge tubes and centrifuged at 8000rpm for 30s
7. Poured off supernatant and resuspended cell pellet in 5ml of cold 50mM CaCl ₂ .		7. Poured off the supernatant and resuspended in .5ml of col 30mM CaCl ₂
8. Cell suspension was incubated on ice for 30 min		8. Transferred 50µl of cell suspension and 2µl of ligation mixture to 1.5ml microcentrifuge tubes
9. Cell suspension was centrifuged at 5,000 rpm for 10min at 4°C		9. Heat shocked at 42°C for 30s and then immediately place on ice for 5 min
10. Poured of supernatant and resuspended the cell pellet in 1ml		10. Transferred contents of the microcentrifuge tubes to glass

of 50mM CaCl ₂		culture tubes that contained 1ml of LB broth
11. Transferred 200µl of cell suspension to a pre-chilled glass culture tube		11. Incubated culture for 1 hour in shaker incubator set at 37°C and 250rpm
12. Added 5µl of ligation mixture to the cell suspension and heat shocked at 42°C for 2 min		12. Transferred and spread full volume onto LB/AMP agar plates
13. Added 800µl of LB broth to the culture tube and incubated for 45 min in a shaker incubator set at 37°C and 250rpm		
14. Transferred and spread 100µl of the cell solution onto LB/AMP agar plates		

Table 4 Electroporation protocols tested for transformation of *E. coli* with sgRNA/Cas9/pTREX-n ligation solutions.

Electroporation transformation protocol (Third protocol tested for <i>pfr2</i>sgRNA/Cas9/pTREX-n plasmid transformation)	Modifications to electroporation transformation protocol (Fourth protocol tested for <i>pfr2</i>sgRNA/Cas9/pTREX-n plasmid transformation)	Further modification to electroporation transformation protocol (Fifth protocol tested for <i>pfr2</i>sgRNA/Cas9/pTREX-n plasmid transformation and first protocol tested for <i>pfr5</i>sgRNA/Cas9/pTREX-n plasmid transformation)
1. Inoculated 3ml of LB broth with a single colony of JM109	1. Inoculated 3ml of LB broth with a single colony of HB101	10. Transferred 40µl of cell suspension and 5µl of ligation mixture to pre-chilled cuvettes
2. Incubated inoculated culture overnight in a shaking incubator set at 37°C and 250rpm	7. Poured off supernatant and resuspended cell pellet in 10ml of 10% glycerol	11. Using the BTX ECM 830 electroporator 1 pulse set 400v and 15s was applied to one cuvette and 1 pulse set at 2,500v and 90µs was applied to another. Following electroporation 1ml of LB was added to the cuvettes and the contents of the cuvettes were transferred to glass culture tubes. The culture tubes were then place in a shaking incubator set at 37°C and 250rpm, for 1 hour.
3. Inoculated 25ml of LB broth with 100µl of overnight culture	10. Transferred 40µl of cell suspension and 2µl of ligation mixture to pre-chilled cuvettes	
4. Incubated culture for 3 hours in a shaking incubator set at 37°C and 150rpm	11. Using the BTX ECM 830 electroporator 1 pulse set 400v and 15s was applied to one cuvette and 1 pulse set at 1,800v and 5ms was applied to another. Following electroporation 1ml of LB was added to the cuvettes and the contents of the cuvettes were transferred to glass culture tubes. The culture tubes were then place in a shaking incubator set at 37°C and 250rpm, for 30 min.	
5. Incubated culture on ice for 30 min	12. 100µl of the cultures was transferred and spread onto LB/AMP agar plates	

6. Transferred chilled culture to a pre-chilled 50ml conical tube and centrifuged at 5,000rpm for 10min at 4°C
7. Poured off supernatant and resuspended cell pellet in 10ml of 50% glycerol
8. Centrifuged cells at 5,000rpm for 10min at 4°C
9. Poured off supernatant and resuspended cell pellet in remaining liquid
10. Transferred 40µl of cell suspension and 1µl of ligation mixture to pre-chilled cuvettes
11. Applied 1 pulse to the cuvette using the BTX ECM 830 electroporator set at 400v and 15s
12. The entire volume of the cuvettes were transferred and spread onto LB/AMP agar plates

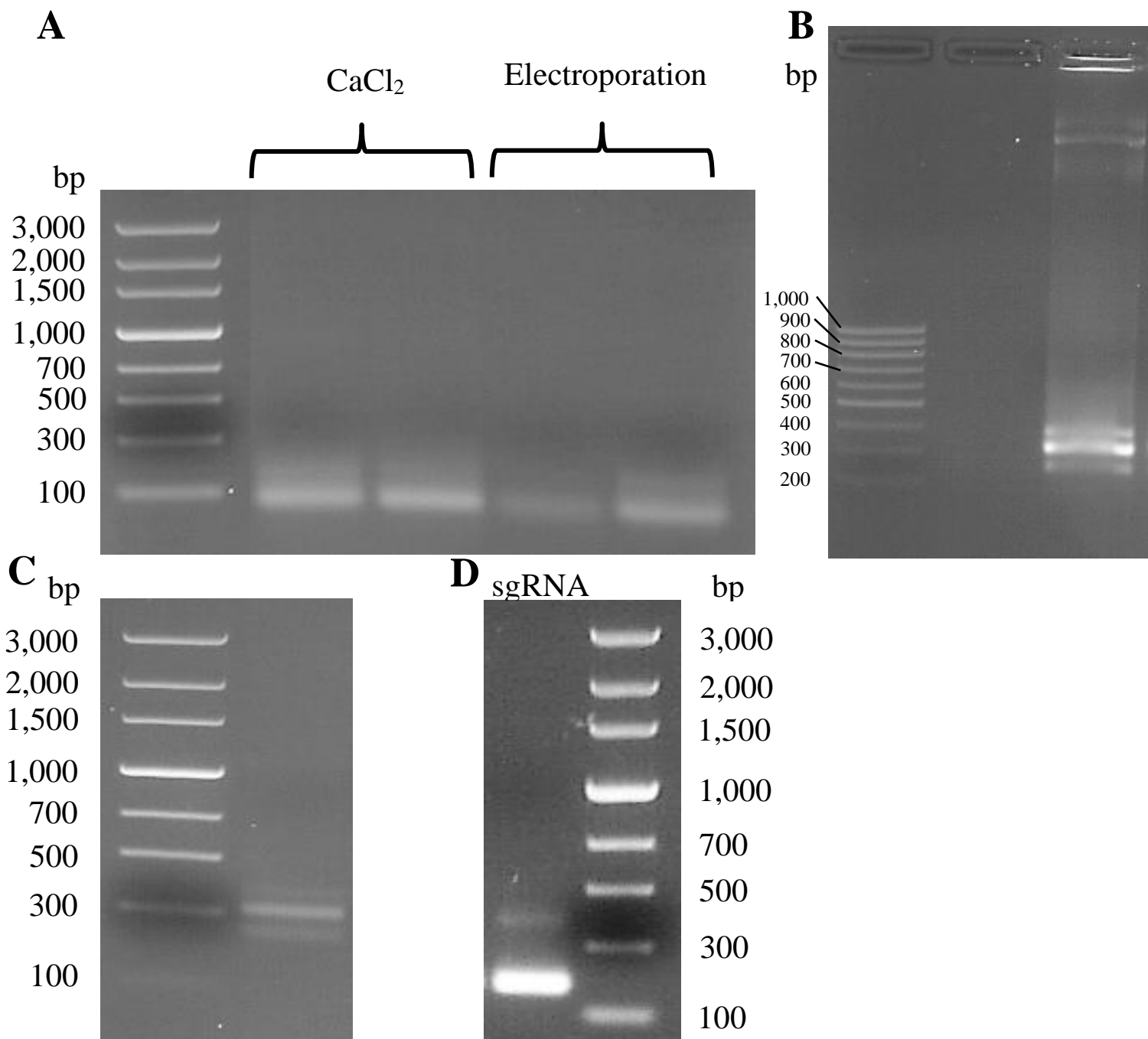


Figure 9 Agarose gel electrophoresis images showing the results of the PCRs done to confirm presence sgRNA/Cas9/pTREX-n plasmid in the bacterial colonies from the various transformation protocols tested. (A) Colony PCR of the colonies produced by the modified CaCl₂ and the electroporation protocol (Table 2, column 2; Table 3 column 1). (B) Representative image showing PCR of plasmid DNA from colonies produced by the further modified electroporation protocol (Table 3, column 3). (C) PCR of plasmid DNA from the colony produced by the 2nd CaCl₂ protocol (Table 2, column 3). (D) Representative image showing the PCR of plasmid DNA from colonies produced by the CaCl₂ protocol described within the methods. Expected size was 190bp.

A

Expected AAAGCGCCGTGTGGATGCCAAGTCTGTGCAAGAGTTCTAGT**GGATCC**TGGGTGGCACCGG
PFR2 Plasmid AAAGCGCCGTGTGGATGCCAAGTCTGTGCAAGAGTTCTAGTGGATCCTGGGTGGCACCGG

Expected CGGACAC**GTTTTAGAGCTAGAAATAGCAAGTTAAAATAAGGCTAGTCCGTTATCAACTTG**
PFR2 Plasmid CGGACACGTTTTAGAGCTAGAAATAGCAAGTTAAAATAAGGCTAGTCCGTTATCAACTTG

Expected **AAAAAGTGGCACCGAGTCGGTGC**TTTTTT**GGATCC**CCCAACGAG
PFR2 Plasmid AAAAAGTGGCACCGAGTCGGTGCTTTTTTGGATCCCAACGAG

B

Expected GCCGTGTGGATGCCAAGTCTGTGCAAGAGTTCTAGT**GGATCC**GACTAAAGAGCCTCCTCG
PFR5 Plasmid GCCGTGTGGATGCCAAGTCTGTGCAAGAGTTCTAGTGGATCCGACTAAAGAGCCTCCTCG

Expected TGGTTTTAGAGCTAGAAATAGCAAGTTAAAATAAGGCTAGTCCGTTATCAACTTGAAAAA
PFR5 Plasmid TGGTTTTAGAGCTAGAAATAGCAAGTTAAAATAAGGCTAGTCCGTTATCAACTTGAAAAA

Expected **GTGGCACCGAGTCGGTGC**TTTTTT**GGATCC**CCCAACGAG
PFR5 Plasmid GTGGCACCGAGTCGGTGCTTTTTTGGATCCCAACGAG

Figure 10 Clustal omega DNA sequence alignments of sgRNA/Cas9/pTREX-n plasmids for (A) *pfr2* and (B) *pfr5*. Bolded sequences are BamHI restriction sites, underlined sequences are guide sequences, red sequences are tracrRNA, and asterix indicate matching nucleotides.

Donor DNA

Construction of the donor DNA cassette used for gene tagging started with selection of the homology arms. Cas9 endonuclease cuts 3nt upstream of the PAM site, so 30nt (for *pfr5* gene tagging) or 100nt (for *pfr2* gene tagging) long sequences on either side of the break were chosen as homology arms. Both lengths were chosen to test if a shorter length could be used for this type of gene tagging protocol and due to the high cost of long primers. The sequences for the homologous arms were incorporated into forward and reverse primers (Table 1, Primers 5-8) that were used to amplify the pMOTag-2H plasmid. This plasmid contained a 3x hemagglutinin (HA) tag, a tubulin intergenic region (*tigr*), and a puromycin resistance gene. Several different PCR reactions

mixtures and thermocycler programs were utilized throughout the creation of donor DNA, with all of them providing bright bands at the expected size (1.3kB – *pfr2*, 1.1kB – *pfr5*) (figure 11). The reason for the different PCR set ups was to increase DNA yield while decreasing the amount of primer used. The first PCR set up included at 50µl PCR reaction with 25µl Q5 high-fidelity 2x master mix, 30ng pMOTag2H, 2µl DMSO, nanaopure H₂O, and 0.8µM forward and reverse primer (Table 1, primers 5 and 6). The PCR conditions were: initial denaturation at 98°C for 2min, followed by 30 cycles of 98°C for 20s, 63°C for 20s, and 72°C for 1 min 20s, followed by a final extension at 72°C for 10 min. This PCR set up was only used for *pfr2* donor DNA amplification and all resulting PCR product was run on an agarose gel a recovered using the Zymo gel DNA recovery kit. The next PCR set up used included a 40µl PCR reaction with 25µl Q5 high-fidelity 2x master mix, 30ng pMOTag2H plasmid, 2µl DMSO and 0.4µM forward and reverse primer (Table 2, primers 5-8). The set up was used for both *pfr2* and *pfr5* donor DNA amplification and used the PCR conditions from the methods section. The main difference between this set up and the prior is the decrease in the amount of primer used and the use of a DNA clean and concentrator kit rather than the gel recovery kit. Prior to using the clean and concentrator kit a small volume (about 5µl) of PCR product was run on an agarose gel to confirm correct amplification. The use of the DNA clean and concentrator allowed for higher DNA yield from the PCR reactions. The final PCR set up used is the one described within the methods, with the only difference from the

prior set up being the increase in reaction volume from 40 μ l to 50 μ l. This increase was done to increase in DNA yield.

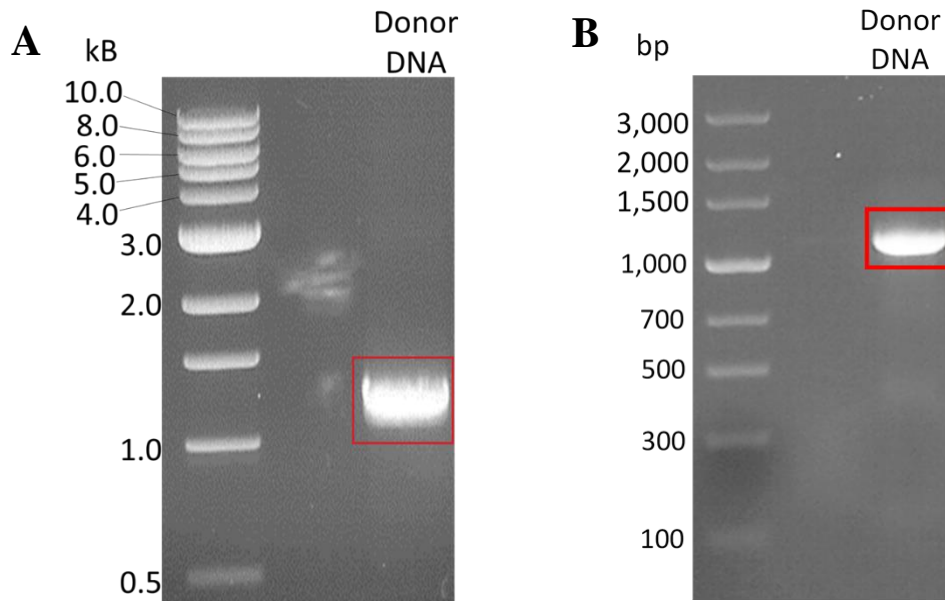


Figure 11 Representative agarose gel electrophoresis images of donor DNA amplification for gene tagging of (A) *pfr2* and (B) *pfr5*. Expected sizes of 1.3kB (A)

Transfections and Antibiotic Selection

Four transfection and antibiotic selection protocols were tested throughout this study with the final protocol, which is detailed in the methods section, being the most successful, in terms of the length of parasite survival post transfection. The first protocol tested started with the growth of *T. cruzi* epimastigotes to a concentration of $1-2 \times 10^7$ cells/ml. Once the parasite reached this concentration, they were transferred to a 15ml conical tube and centrifuged at 2,000 rpm for 5 min. The supernatant was then poured off and the cell pellet was washed by resuspending the pellet in 5ml of PBS and centrifuging at 2,000 rpm for 5 min. The supernatant was again poured off and the cells were resuspended in cold cytomix (120mM KCl, .15mM CaCl₂, 25mM HEPES, 2mM EDTA, and 5mM MgCl₂) at a concentration of 1×10^8 cells/ml. This cell suspension was then

transferred to pre-chilled cuvettes, along with *pfr2* specific plasmid and donor DNA, according to the layout presented in table 5. Once everything had been added to the cuvettes, they were placed on ice to 10 min. After incubating on ice, the BTX ECM 830 electroporator was used to deliver three electrical pulses at 1030v/90 μ s to each cuvette. Between each pulse, the cuvettes were placed on ice for 1 min. Following the completion of the three pulses, the cuvettes were placed at room temperature for 15 min to allow the cells to recover. The entire volume of the cuvettes was then transferred to culture flasks that contained 5ml of Schneider's complete medium with 20% FCS. 24 hours after transfection 250 μ g/ml G418 (selects for the plasmid) and 5 μ g/ml puromycin (selects for the donor DNA) was added to the flasks. The media was changed out every week by transferring the contents of the flask to 15ml conical tube and centrifuging them at 700rpm for 5 min. Most of the parasites died off within the first week after transfection, with very few still alive in the following weeks. Many of the parasites that survived after the initial decline in population had decreased flagellar movement compared to wild type parasites.

The next protocol tested, used the prior protocol as a foundation, with the addition of several modifications. These modifications included a change in centrifuge speed and time (2,000rpm/5min to 1,200rpm for 10min), a decrease in the volume of cells used for each transfection (400 μ l to 350 μ l), and a change in how the cells were cultured post transfection. The decrease in parasite volume was done in the hopes to decrease the overall volume in the cuvettes and increase the max voltage that could be applied the cuvettes. The voltage did slightly increase from the prior transfections done, from 1030v/90 μ s to 1056v/101 μ s. For culturing post transfection, 24 hours after transfection

the contents of the culture flasks were transferred to 15ml conical tubes and centrifuged at 1250rpm for 10 min. The supernatant was then poured off and the cells were resuspended in Schneider's medium with antibiotics. This protocol of centrifuging the parasite and resuspending them in fresh media was repeated once a week for three weeks. After the three weeks, the contents of the flasks transfected with *pfr2* plasmid and donor DNA (transfection layout in table 6) were transferred to 24 well plates, with 1 ml per well. This was done to allow for easier spotting of the parasites under the inverted microscope. Fresh media was either added directly to the well or the top half of the existing media was removed, and fresh media was added to replace it. Over the course of the next few weeks, several of the wells still had clusters of surviving parasites that had good flagellar movement. These clusters would not grow frequently and would occasionally decrease in populations numbers. This trend continued until it was decided to move on to a new transfection, due to low parasite numbers.

The next protocol tested built upon the prior protocol with a few modifications. These modifications included a decrease in cell concentration (1×10^8 to 2.27×10^7 cells/ml), a decrease in G418 added post transfection (250 to $100 \mu\text{g/ml}$), and a change in cell culturing post transfection. The change in cell concentration was due to the 1×10^8 cells/ml concentration not producing the volume necessary to perform all of the transfections required (layout in table 7), while the change in G418 concentration was done to see if cell viability would increase. For culturing post-transfection, 24 hours after transfection the contents of the culture flasks were transferred to 15 ml conical tubes, diluted (1:2 and 1:4), and transferred to 96 well plates ($200 \mu\text{l}$ per well) (figure 12). Half of the media was removed each week and replaced with fresh media with antibiotics.

Within a few weeks after transfection, most of the parasites transfected with *pfr5* plasmid and donor DNA had died and no parasite clusters (sign of population growth) could be seen.

The final protocol performed was the one detailed in the methods section. Similar to the other protocol this one built off the prior with modifications. The main modifications implemented during this protocol included an increase in voltage (1056v/101 μ s to 1340v/100 μ s), change in electroporation buffer used (cytomix to Tb-BSF), and a change in culturing techniques post transfection (figure 5). The increase in voltage was accomplished through decreasing the volume of plasmid and donor DNA that needed to be added to the cuvettes, which allowed for a decrease in the total volume within the cuvettes (table 2). This decrease in plasmid and donor DNA volume was accomplished through increased efficiency during miniprep and ethanol precipitation procedures. The change in electroporation buffers was done to help decrease cell death immediately following transfection. This decrease in cell death was seen during this round of transfections, with both the control cells and the plasmid and donor DNA transfected cells having either minimal cell death or less cell death compared to cytomix, 24 hours post transfection. This protocol was our most successful in terms of cell viability post transfection with parasites showing signs of cell growth six plus weeks after transfection. These signs of cell growth were only seen with the parasites transfected with *pfr2* plasmid and donor DNA, while those transfected with *pfr5* plasmid and donor DNA saw continuously dwindling populations over the course of several weeks. Although the *pfr2* transfected parasites did show positive signs of growth they never reached numbers comparable to those seen when culturing wild type *T. cruzi*.

Table 5 Set up of the four cuvettes used during the first transfection protocol tested.

<i>Pfr2</i> transfection	<i>Pfr2</i> transfection	Control	Control
40µl <i>pfr2</i> sgRNA/Cas9/pTREX-n plasmid (28µg)	26µl <i>pfr2</i> sgRNA/Cas9/pTREX-n plasmid (10µg)	10µl nanopure H ₂ O	400µl (1x10 ⁸ /ml Epimastigotes)
80µl <i>pfr2</i> donor dna (15µg)	30.5µl <i>pfr2</i> donor dna (8µg)	400µl (1x10 ⁸ /ml Epimastigotes)	
400µl (1x10 ⁸ /ml Epimastigotes)	400µl (1x10 ⁸ /ml Epimastigotes)		

Table 6 Set up of the four cuvettes used during the second transfection protocol tested.

<i>Pfr2</i> transfection	<i>Pfr2</i> transfection	Control	Control
137µl donor dna (24.9µg)	106µl donor dna (18.1µg)	10µl nanopure H ₂ O	350µl 1x10 ⁸ cells/ml epimastigotes
128µl sgRNA/Cas9/pTREX-n plasmid (23.3µg)	128µl sgRNA/Cas9/pTREX-n plasmid (25.2µg)	350µl 1x10 ⁸ cells/ml epimastigotes	
350µl 1x10 ⁸ cells/ml epimastigotes	350µl 1x10 ⁸ cells/ml epimastigotes		

Table 7 Set up of the three cuvettes used during the third transfection protocol tested.

<i>Pfr5</i> transfection	sgRNA/Cas9 plasmid control	Control
129µl donor dna (26.71µg)	116µl sgRNA/Cas9/pTREX-n plasmid (26µg)	400µl 2.27x10 ⁷ cells/ml epimastigotes
116µl sgRNA/Cas9/pTREX-n plasmid	400µl 2.27x10 ⁷ cells/ml epimastigotes	
400µl 2.27x10 ⁷ cells/ml epimastigotes		

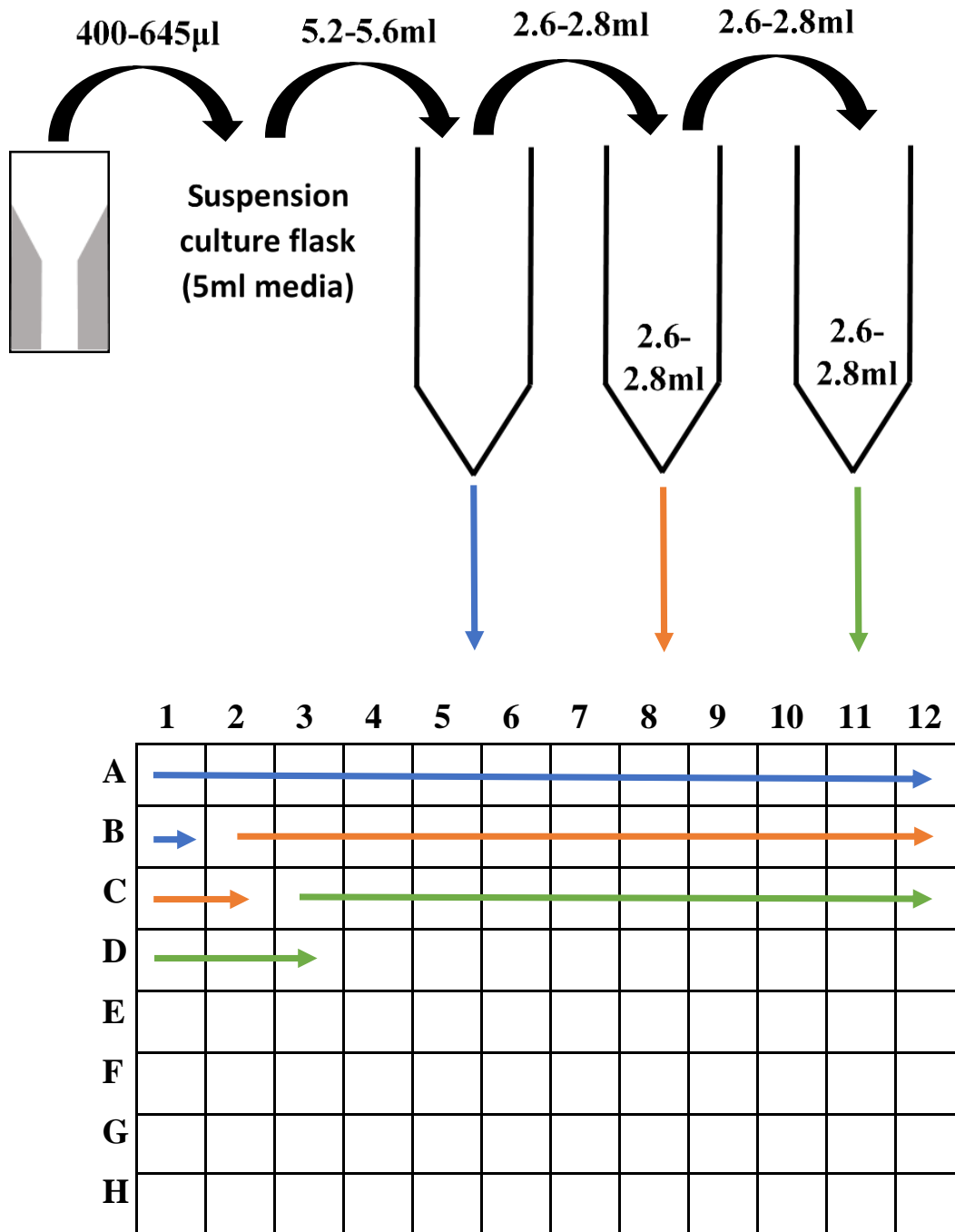


Figure 12 Illustration detailing how all the transfections from table 7 were diluted and plated 24 hours post transfection.

Transfection Confirmation

Integration of *pfr2* specific sgRNA/Cas9/pTREX-n plasmid and donor DNA cassette, during implementation of transfection and antibiotic selection protocols two and four, was tested periodically after the antibiotic selection was started. Genomic DNA from possibly double resistant mutants was used to PCR amplify the sgRNA from the plasmid [*pfr2* guide sequence forward primer and HX1 reverse primer (Table 1, Primers 1 and 4)] and the donor DNA cassette insert [gene specific forward primer and puromycin resistance gene reverse primer (Table 1, Primers 10 and 9)]. Genomic DNA from second protocol was isolated using the Wizard SV genomic DNA purification system (Promega, ca# A2360) rather than the method described in the methods section. Only the sgRNA showed amplification at the expected size of 190bp (figure 13). PCR confirmation of integration was not done for the first protocol, third protocol, and *pfr5* transfects from the fourth protocol, due to the low number of viable parasites and the inability to obtain a sufficient amount of genomic DNA for analysis.

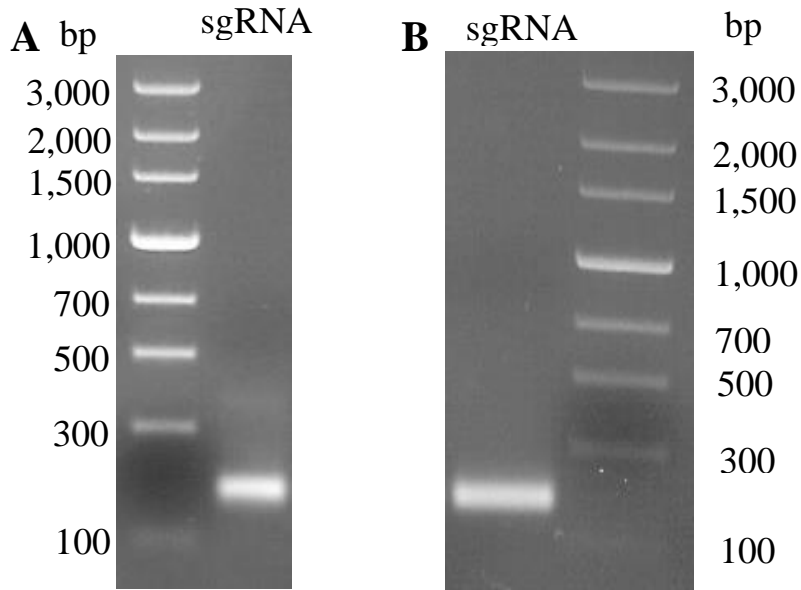


Figure 13 Representative agarose gel electrophoresis images showing the amplification of *pfr2* sgRNA from genomic DNA of parasites transfected with *pfr2* sgRNA/Cas9pTREX-n plasmid and donor DNA cassette. (A) From parasites transfected using the second transfection and antibiotic selection protocol. (B) From parasites transfected using the fourth transfection and antibiotic selection protocol. Expected size of 190bp.

CHAPTER V

DISCUSSION

Within this study, we were able to create plasmid and DNA constructs for *pfr2* and *pfr5* gene tagging, as well as confirm the incorporation of *pfr2* specific sgRNA/Cas9/pTREX-n plasmid into the genome. In addition, we were able to rework and troubleshoot much of the protocol from Lander et al. (2016) to function within our lab. Much of the troubleshooting was with the bacterial transformation following ligation and with maintenance of viable epimastigotes post transfection. While the bacterial transformation was successfully troubleshoot through the testing and modification of several CaCl₂ and electroporation protocols, the survivability and growth of epimastigotes post transfection is still a work in progress. Throughout the different transformation and antibiotic selection, protocols tested a consistent problem was a lack of or stunted parasite growth. In some instances, such as some of the *pfr2* transfected parasites from the second and fourth protocols, parasite clusters that contained parasites with normal flagellar movement could be seen, but these parasite clusters never grew to sizes seen with wild type *T. cruzi*. The *pfr5* transfected parasites rarely showed signs of the clusters and often died off in greater numbers before the *pfr2* transfected parasites. In addition to the lack of growth, PCR amplification of *pfr2* donor DNA from genomic DNA never produced PCR product, even though there were viable parasites up to 6 plus weeks post transfection.

The lack of integration or confirmation of integration could be due to variety of factors that have yet to be fully explored, although a few reason could be the inefficiency of the parasites to go through HDR, the length of the homologous arms (in the case of

pfr5) not being long enough for HDR in *T. cruzi* or, the cell debris present within the media limiting growth. In regard to the efficacy of the repair mechanism, when the DNA of the parasite is cut by the sgRNA/Cas9 complex the break will most often be repaired using NHEJ since this is often a less intensive process that does not require the use of a homologous sequence, thus limiting the likelihood that donor DNA will be used for repair. The length of the homologous arms for the *pfr5* donor DNA cassette is the most probable reason as to why the *pfr5* transfected parasites fared worse than the *pfr2* transfected parasites. The decision to try the smaller 30bp (compared to 100bp) homologous arms was spurred by a publication that utilized this arm length to tag genes with mNeonGreen, make null mutants using resistance genes and switch out fluorescent reporter proteins in *T. cruzi* (Costa et al., 2018). Although this publication was able to use a smaller arm length, our implementation of the 30bp homologous arms resulted in the *pfr5* transfected parasites having visibly fewer numbers post-transfection than the *pfr2* transfected. In addition, those parasites often had decreased flagellar movement. These observations suggest that the length of the homology arms plays an important role in the likelihood of HDR. It is possible that for the length of our donor DNA cassette, longer homologous arms were necessary and the use of longer homology arms with the *pfr2* transfections may have contributed to their prolonged survival. In the weeks after transfection, a large portion of the parasites died, thus leaving a lot of cell debris in the media. When changing out the media in the few weeks following transfection, several centrifuge speeds were tested to see if this would limit the amount of debris that would be carried over. A lower centrifuge speed did seem to get rid of some of the debris but much of it remained. Another problem with the debris is that the parasite would often get suck

in the debris, leaving very few free-swimming parasites. The parasites did seem to be able to divide when stuck within the debris although the growth was limited.

An additional factor that could explain the low number of parasites, but could also limit the use of this protocol, is the possibility that the gene tagging protocol is resulting in a fatal mutation. The PFR is a trilaminar structure composed of cytoskeletal filaments that come together to form one cohesive structure, that works to provide stability to the flagellum (Portman and Gull, 2010). The exact way in which the various proteins of the PFR interact and/or bind to one another is not fully understood, although knockout studies have been performed to investigate the importance of various PFR proteins in the overall function of the PFR. One such study knocked out two of the core proteins of the PFR, PFR1, and PFR2, by using CRISPR/Cas9 to insert an antibiotic resistance gene at the N-terminus of the genes (Lander et al., 2015). Knockouts of either protein resulted in an incomplete formation of the PFR, detachment of the axoneme from the cellular body, and a loss of motility (Lander et al., 2015). In essence, the disruption of *pfr1* or *pfr2* resulted in a lethal mutation. The results of this study could be an indicator as to why our parasite populations were always so low. The insertion of the tag sequence at the C-terminus of the genes, particularly *pfr2*, could have hindered the ability of the proteins to correctly incorporate into the PFR to some extent and resulted in a fatal mutation, similar to that of the study. Further testing needs to be done to determine if this is occurring or if there is another reason behind the low cell populations. If tagging of *pfr* genes is a lethal mutation, then this protocol may not be viable for PFR localization even though it has been successfully used in the localization of a flagellar calcium binding protein and acidocalcisome vacuolar proton pyrophosphatase in *T. cruzi* (Lander et al., 2016).

As stated earlier there were changes made to the original Lander et al. (2016) protocol, with those changing including: reagents used for PCR and PCR product cleanup (i.e. Q5 high fidelity 2x master mix, Apex Taq RED master mix, Zymo gel DNA recovery kit, and DNA clean and concentrator kit), length of homology arms for donor DNA cassette (from 100bp to 30bp for *pfr5* tagging), culture medium (Schneider's complete media instead of liver infusion tryptose), electroporation conditions (1.3kV, 100 μ s instead of 1.5kV, 25 μ F; the use of Tb-BSF instead of cytomix), and several aspects of the various protocols detailed in the methods and results sections. Some of these changes were done out of necessity (i.e. limited budget or supplies available; Q5 high fidelity 2x master mix, Apex Taq RED master mix, and Schneider's complete media, electroporator settings) while others were done to test the viability of different methods (DNA clean and concentrator kit, length of homologous arms, and electroporation conditions). The implementation of the DNA clean and concentrator kit and the electroporation conditions resulted in some of the most positive differences when testing out all of the various methods. The clean and concentrator consistently allowed us to get higher DNA yield from our PCRs in comparison to the Zymo gel recovery kit, while the Tb-BSF resulted in less cell death immediately following electroporation in comparison to cytomix. The decision to use Tb-BSF rather than cytomix for the final round of transfections was spurred by a study done by Romagnoli et al. (2018), which aimed to improve CRISPR/Cas9 gene disruption in *T. cruzi*. Within this study, they tested out various electroporation solutions, including Tb-BSF and cytomix, and compared cell viability post-transfection. The results of these tests showed that cytomix was the worst performing, with ~15% viability 24 hours post-transfection, while Tb-BSF was one of the

best performing, with ~90% viability 24 hours post-transfection (Romagnoli et al., 2018). A similar difference in cell viability was seen within our final transfection and was most notable with the control cells, which had minimal cell death 24 hours post transfection, but could also be seen with the *pfr2* and *pf5* transfected cells, which has less cell debris than what was common with cytomix 24 hours post transfection. We were only able to test this buffer during a single round of transfection, but from what was seen during this transfection and the Romagnoli et al. (2018) publication it seems that this buffer is preferable for *T. cruzi* electroporation. While the change in electroporation buffer was driven by a literature search, the decrease in voltage used for electroporation was due to the limits of the electroporator used within our study. Through the various transfection protocols tested the electroporator was initially set to 1.5kV but it was unable to deliver this voltage because of arching, which can be due to the presence of air bubbles or high concentration of salts. Although we were not able to reach the voltage designated in the Lander et. al (2016), we were able to get close by decreasing the volume of plasmid and donor DNA added to the cuvette. A further decrease in volume may increase the charge that can be delivered and potentially have a slight impact on transfection efficiency.

In order to move past the current hurdle of parasite viability and obtain gene tagged parasites, we are continuing to investigate ways to improve transfection efficiency, in addition to looking into other CRISPR protocols that have been developed with *T. cruzi*. Means by which to improve transfection efficiency could include, performing multiple transfections on the same cell population, which increases the likelihood that a parasite will integrate both the plasmid and the donor DNA, or using products that increase HDR likelihood, such as the IDT HDR enhancer (cat# 1081072).

Regarding other CRISPR protocols for *T. cruzi*, one protocol, presented in Romagnoli et al (2018), first established a stable cell line that expresses Cas9-GFP using the Cas9/pTREX-n plasmid and then transfected with transcribed sgRNA. This protocol was only used to test gene knockouts using gene specific sgRNA, but aspects of this protocol could be integrated into the current one to alleviate the requirement that two large constructs, the sgRNA/Cas9/pTREX-n plasmid and the donor DNA, must enter the cell during the same transfection in order for gene tagging to work. Another protocol presented in Soares Medeiros et al. (2017) took the approach of transfecting parasites with a Cas9/sgRNA protein complex (instead of a plasmid) assembled using Cas9 from *S. aureus* (smaller than the commonly used Cas9 from *S. pyogenes*) and donor DNA that contained only 2 HA epitopes flanked by 20bp homology arms. Three days post transfection these parasites were stained with anti-HA antibodies and put through a flow cytometer (Soares Medeiros et al., 2017). Those that were positive for the HA tag were examined under a microscope to look for protein localization (Soares Medeiros et al., 2017). The implementation of a smaller endonuclease and donor DNA could greatly improve our transfection efficiency, while the use of flow cytometry would eliminate the need for antibiotic selection and would allow us to determine if our transfections were successful earlier. In conclusion, the completion of the DNA constructs, as well as the troubleshooting of the procedures used, does provide a foundation for future students to utilize and improve upon this technique.

LITERATURE CITED

- Acevedo GR, Girard MC, Gómez KA. 2018. The unsolved jigsaw puzzle of the immune response in Chagas disease. *Front Immunol.* 9:1929.
- Addgene. 2017. CRISPR 101: a desktop resource. Addgene; [accessed 2019 May 31]. <https://info.addgene.org/download-addgenes-ebook-crispr-101-2nd-edition>
- Albertti LAG, Macedo AM, Chiari E, Andrews NW, Andrade LO. 2010. Role of host lysosomal associated membrane protein (LAMP) in *Trypanosoma cruzi* invasion and intracellular development. *Microbes Infect.* 12(10):784–789.
- Alvarez MN, Peluffo G, Piacenza L, Radi R. 2011. Intraphagosomal peroxynitrite as a macrophage-derived cytotoxin against internalized *Trypanosoma cruzi*: consequences for oxidative killing and role of microbial peroxiredoxins in infectivity. *J Biol Chem.* 286(8):6627-6640.
- Andrews NW, Abrams CK, Slatin SL, Griffiths G. 1990. A *T. cruzi*-secreted protein immunologically related to the complement component C9: evidence for membrane pore-forming activity at low pH. *Cell.* 61(7):1277–1287.
- Bafica A, Santiago HC, Goldszmid R, Ropert C, Gazzinelli RT, Sher AJ. 2006. Cutting edge: TLR9 and TLR2 signaling together account for MyD88-dependent control of parasitemia in *Trypanosoma cruzi* infection. *J Immunol.* 177(6):3515–3519.
- Barrangou R, Fremaux C, Deveau H, Richards M, Boyaval P, Moineau S, Romero DA, Horvath P. 2007. CRISPR provides acquired resistance against viruses in prokaryotes. *Science.* 315(5819):1709–1712.
- Barrangou R, Marraffini LA. 2014. CRISPR-Cas systems: prokaryotes upgrade to adaptive immunity. *Mol Cell.* 54(2);234–244.
- Bartholomeu DC, de Paiva RMC, Mendes TAO, DaRocha WD, Teixeira SMR. 2014. Unveiling the intracellular survival gene kit of trypanosomatid parasites. *PLoS Pathog.* 10(12):e1004399.
- Bern C, Kjos S, Yabsley MJ, Montgomery SP. 2011. *Trypanosoma cruzi* and Chagas' disease in the United States. *Clin Microbiol Rev.* 24(4):655-681.
- Bern, C, Martin, DL, Gilman, RH. 2011. Acute and congenital Chagas disease. In: Weiss, LM, Tanowitz, HB, Kirchhoff, LV, editors. *Advances in parasitology Chagas disease, part A.* Amsterdam: Elsevier p 20-39.

- Bezerra CM, Cavalcanti LP, Souza Rde C, Barbosa SE, Xavier SC, Jansen AM, Ramalho RD, Diotaiuti L. 2014. Domestic, peridomestic and wild hosts in the transmission of *Trypanosoma cruzi* in the Caatinga area colonized by *Triatoma brasiliensis*. Mem Inst Oswaldo Cruz. 109(7):887–898.
- Brenière SF, Bosseno MF, Gastélum EM, Soto Gutiérrez MM, de Jesús Kasten Monges M, Barraza Salas JH, Romero Paredes JJ, de Jesús Lozano Kasten F. 2010. Community participation and domiciliary occurrence of infected *Meccus longipennis* in two mexican villages in Jalisco state. Am J Trop Med Hyg. 83(2):382–387.
- Caetano BC, Carmo BB, Melo MB, Cerny A, dos Santos SL, Bartholomeu DC, Golenbock DT, Gazzinelli RT. 2011. Requirement of UNC93B1 reveals a critical role for TLR7 in host resistance to primary infection with *Trypanosoma cruzi*. J Immunol. 187(4):1903–1911.
- Campos MA, Almeida IC, Takeuchi O, Akira S, Valente EP, Procópio DO, Travassos LR, Smith JA, Golenbock DT, Gazzinelli RT. 2001. Activation of toll-like receptor-2 by glycosylphosphatidylinositol anchors from a protozoan parasite. J Immunol. 167(1):416–423.
- Cardoso MS, Reis-Cunha JL, Bartholomeu DC. 2015. Evasion of the immune response by *Trypanosoma cruzi* during acute infection. Front Immunol. 6:659.
- Centers for Disease Control and Prevention (CDC). 2019-A. Parasites – american trypanosomiasis (also known as Chagas disease): epidemiology & risk factors. [Accessed 2019 May 31]. <https://www.cdc.gov/parasites/chagas/epi.html>
- Centers for Disease Control and Prevention (CDC). 2019-B. Antiparasitic treatment. [accessed 2019 Apr 29]. https://www.cdc.gov/parasites/chagas/health_professionals/tx.html
- Cestari Idos S, Evans-Osses I, Freitas JC, Inal JM, Ramirez MI. 2008. Complement C2 receptor inhibitor trispanning confers an increased ability to resist complement-mediated lysis in *Trypanosoma cruzi*. J Infect Dis. 198(9):1276–1283.
- Cestari Idos S, Krarup A, Sim RB, Inal JM, Ramirez MI. 2009. Role of early lectin pathway activation in the complement-mediated killing of *Trypanosoma cruzi*. Mol Immunol. (2–3):426–437.
- Clark AK, Kovtunovych G, Kandlikar S, Lal S, Stryker GA. 2005. Cloning and expression analysis of two novel paraflagellar rod domain genes found in *Trypanosoma cruzi*. Parasitol Res. 96(5):312–320.

- Costa FC, Francisco AF, Jayawardhana S, Calderano SG, Lewis MD, Olmo F, Beneke T, Gluenz E, Sunter J, Dean S, et al. 2018. Expanding the toolbox for *Trypanosoma cruzi*: a parasite line incorporating a bioluminescence-fluorescence dual reporter and streamlined CRISPR/Cas9 functionality for rapid *in vivo* localization and phenotyping. PLoS Negl Trop Dis. 12(4):e0006388.
- Coura JR, Dias JCP. 2009. Epidemiology, control and surveillance of Chagas disease: 100 years after its discovery. Mem Inst Oswaldo Cruz. 104 Suppl 1:31-40.
- Cunha NL, De Souza W, Hasson-Volovh A. 1984. Isolation of the flagellum and characterization of the paraxial structure of *Herpetomonas megaseliae*. J Submicrosc Cytol. 16(4):705-713.
- de Lana, M, Marques, E, Machado, M. 2010. Biology of *Trypanosoma cruzi* and biological diversity. In: Telleria J, Tibayrenc M. editors. American trypanosomiasis Chagas disease one hundred years of research. Amsterdam: Elsevier. p 339-356.
- de Pablos LM, Osuna A. 2012. Multigene families in *Trypanosoma cruzi* and their role in infectivity. Infect Immun. 80(7):2258–2264.
- Doudna JA, Charpentier E. 2014. The new frontier of genome engineering with CRISPR-Cas9. Science. 346(6213):1258096.
- Farina M, Attias M, Souto-Padron T, de Souza W. 1986. Further studies on the organization of the paraxial rod of trypanosomatids. J Protozool. 33(4):552–557.
- Ferreira V, Valck C, Sánchez G, Gingras A, Tzima S, Molina MC, Sim R, Schwaeble W, Ferreira A. 2004. The classical activation pathway of the human complement system is specifically inhibited by calreticulin from *Trypanosoma cruzi*. J Immunol. 172(5), 3042–3050.
- Fleischmann RD, Adams MD, White O, Clayton RA, Kirkness EF, Kerlavage AR, Bult CJ, Tomb JF, Dougherty BA, Merrick JM, et al. 1995. Whole-genome random sequencing and assembly of *Haemophilus Influenzae* Rd. Science. 269(5223):496-512.
- Fouts DL, Stryker GA, Gorski KS, Miller MJ, Nguyen TV, Wrightsman RA, Manning JE. 1998. Evidence for four distinct major protein components in the paraflagellar rod of *Trypanosoma cruzi*. J Biol Chem. 273(34):21846-21855.
- Hall BF, Webster P, Ma AK, Joiner KA, Andrews NW. 1992. Desialylation of lysosomal membrane glycoproteins by *Trypanosoma cruzi*: a role for the surface neuraminidase in facilitating parasite entry into the host cell cytoplasm. J Exp Med. 176(2):313-325.

- Hegasy G. CRISPR-Cas9, part1. [accessed 2019 May 31].
https://hegasy.de/03_download_en.html
- Hille F, Charpentier E. 2016. CRISPR-Cas: biology, mechanisms and relevance. *Philos Trans R Soc Lond B Biol Sci.* 371(1707):20150496.
- Hyams JS. 1982. The euglena paraflagellar rod: structure, relationship to other flagellar components and preliminary biochemical characterization. *J Cell Sci.* 55:199-210.
- Ishino Y, Shinagawa H, Makino K, Amemura M, Nakata A. 1987. Nucleotide sequence of the iap gene, responsible for alkaline phosphatase isozyme conversion in *Escherichia coli*, and identification of the gene product. *J Bacteriol.* 169(12):5429-5433.
- Jansen AM, Roque, ALR, 2010. Domestic and wild mammalian reservoirs. In Telleria, J, Tibayrenc, M. editors. *American trypanosomiasis Chagas disease one hundred year of research.* Amesterdam: Elsevier, p 249-270.
- Jansen R, Embden JD, Gaastra W, Schouls LM. 2002. Identification of genes that are associated with DNA repeats in prokaryotes. *Mol Microbiol.* 43(6):1565–1575.
- Joiner KA, Dias W, Rimoldi MT, Hammer CH, Sherii A, Kipnisell TL. 1988. Biochemical characterization of a factor produced by trypomastigotes of *Trypanosoma cruzi* that accelerates the decay of complement C3 convertases. *J Biol Chem.* 263(23):11327-11335.
- Junqueira C, Caetano B, Bartholomeu DC, Melo MB, Ropert C, Rodrigues MM, Gazzinelli RT. 2010. The endless race between *Trypanosoma cruzi* and host immunity: lessons for and beyond Chagas disease. *Expert Rev Mol Med.* 12:e29.
- Ka D, Jang DM, Han BW, Bae E. 2018. Molecular organization of the type II-A CRISPR adaptation module and its interaction with Cas9 via csn2. *Nucleic Acids Res.* 46(18):9805-9815.
- Kornfeld S, Mellman I. 1989. The biogenesis of lysosomes. *Annu Rev Cell Biol.* 5:483-525.
- Kropf SP, Sá MR. 2009. The discovery of *Trypanosoma cruzi* and Chagas disease (1908-1909): tropical medicine in Brazil. *Hist Cienc Saude Manguinhos.* 16 Suppl 1:13-34.
- Kurup SP, Tarleton RL. 2014. The *Trypanosoma cruzi* flagellum is discarded via asymmetric cell division following invasion and provides early targets for protective CD8⁺ T cells. *Cell Host Microbe.* 16(4):439-449.

- Lander N, Li ZH, Niyogi S, Docampo R. 2015. CRISPR/Cas9-Induced disruption of paraflagellar rod protein 1 and 2 genes in *Trypanosoma cruzi* reveals their role in flagellar attachment. *MBio*. 6(4):e01012.
- Lander N, Chiurillo MA, Storey M, Anibal X, Vercesi AE, Docampo R. 2016. CRISPR/Cas9-mediated endogenous c-terminal tagging of *Trypanosoma cruzi* genes reveals the acidocalcisome localization of the inositol 1,4,5-trisphosphate receptor. *J Biol Chem*. 291(49):25505-25515.
- Lidani KCF, Bavia L, Ambrosio AR, de Messias-Reason IJ. 2017. The complement system: a prey of *Trypanosoma cruzi*. *Front Microbiol*. 8:607.
- Makarova KS, Grishin NV, Shabalina SA, Wolf YI, Koonin EV. 2006. A putative RNA-interference-based immune system in prokaryotes: computational analysis of the predicted enzymatic machinery, functional analogies with eukaryotic RNAi, and hypothetical mechanisms of action. *Biol Direct*. 1:7.
- Makarova KS, Wolf YI, Alkhnbashi OS, Costa F, Shah SA, Saunders SJ, Barrangou R, Brouns SJ, Charpentier E, Haft DH, et al. 2015. An updated evolutionary classification of CRISPR-Cas systems. *Nat Rev Microbiol*. 13(11):722-736.
- Martins AV, Gomes AP, Gomes de Mendonça E, Lopes Rangel Fietto J, Santana LA, de Almeida Oliveira MG, Geller M, de Freitas Santos, Vitorino RR, Siqueira-Batista R. 2012. Biology of *Trypanosoma cruzi*: An update. *Infectio*, 16(1), 45-58.
- Miller MJ, Wrightsman RA, Stryker GA, Manning JE. 1997. Protection of mice against *Trypanosoma cruzi* by immunization with paraflagellar rod proteins require T cell but not B cell function. *J Immunol*, 158(11) 5330-5337.
- Mir A, Edraki A, Lee J, Sontheimer EJ. 2018. Type II-C CRISPR-Cas9 biology, mechanism, and application. *ACS Chem Biol*. 13(2):357-365.
- Mojica FJ, Juez G, Rodriguez-Valera F. 1993. Transcription at different salinities of *Haloferax mediterranei* sequences adjacent to partially modified PstI sites. *Mol Microbiol*. 9(3):613-621.
- Mojica FJ, Ferrer C, Juez G, Rodriguez-Valera F. 1995. Long stretches of short tandem repeats are present in the largest replicons of the archaea *Haloferax mediterranei* and *Haloferax volcanii* and could be involved in replicon partitioning. *Mol Microbiol*. 17(1):85-93.
- Mojica FJ, Díez-Villaseñor C, Soria E, Juez G. 2000. Biological significance of a family of regularly spaced repeats in the genomes of archaea, bacteria and mitochondria. *Mol Microbiol*. 36(1):244-246.

- Mojica FJ, Diez-Villasenor C, Garcia-Martinez J, Soria E. 2005. Intervening sequences of regularly spaced prokaryotic repeats derive from foreign genetic elements. *J Mol Evol.* 60(2): 174-182.
- Mojica FJ, Rodriguez-Valera F. 2016. The discovery of CRISPR in archaea and bacteria. *FEBS J.* 283(17):3162-3169.
- Moriya H. 2015. Quantitative nature of overexpression experiments. *Mol Biol Cell.* 26(22):3932-3939
- Mucci J, Hidalgo A, Mocetti E, Argibay PF, Leguizamon MS, Campetella O. 2002. Thymocyte depletion in *Trypanosoma cruzi* infection is mediated by trans-sialidase-induced apoptosis on nurse cells complex. *Proc Natl Acad Sci USA.* 99(6):3896-3901.
- Muñoz-Fernández MA, Fernández MA, Fresno M. 1992. Activation of human macrophages for the killing of intracellular *Trypanosoma cruzi* by TNF- α and IFN- γ through a nitric oxide-dependent mechanism. *Immunol Lett.* 33(1):35-40.
- Nakata A, Amemura M, Makino K. 1989. Unusual nucleotide arrangement with repeated sequences in the *Escherichia coli* K-12 chromosome. *J Bacteriol.* 171(6):3553-3556.
- Norris KA, Bradt B, Cooper NR, So M. 1991. Characterization of a *Trypanosoma cruzi* C3 binding protein with functional and genetic similarities to the human complement regulatory protein, decay-accelerating factor. *J Immunol.* 147(7):2240-2247.
- Oliveira AC, Peixoto JR, de Arruda LB, Campos MA, Gazzinelli RT, Golenbock DT, Akira S, Previato JO, Mendonca-Previato L, Bellio M. 2004. Expression of functional TLR4 confers proinflammatory responsiveness to *Trypanosoma cruzi* glycoinositolphospholipids and higher resistance to infection with *T. cruzi*. *J Immunol.* 173(9):5688-5696.
- Padilla AM, Simpson LJ, Tarleton RL. 2009. Insufficient TLR activation contributes to the slow development of CD8+ T Cell responses in *Trypanosoma cruzi* infection. *J Immunol.* 183(2):1245-1252.
- Piacenza L, Peluffo G, Alvarez MN, Kelly JM, Wilkinson SR, Radi R. 2008. Peroxiredoxins play a major role in protecting *Trypanosoma cruzi* against macrophage- and endogenously-derived peroxynitrite. *Biochem J.* 410(2):359-368.
- Portman N, Gull K. 2010. The paraflagellar rod of kinetoplastid parasites: from structure to components and function. *Int J Parasitol.* 40(2):135-148.

- Pourcel C, Salvignol G, Vergnaud G. 2005. CRISPR elements in *Yersinia pestis* acquire new repeats by preferential uptake of bacteriophage DNA, and provide additional tools for evolutionary studies. *Microbiology*. 151(Pt 3):653-663.
- Radi R. 2013. Peroxynitrite, a stealthy biological oxidant. *J Biol Chem*. 288(37):26464-26472.
- Rassi, A, de Rezende, JM, Luquetti, AO, Rassi, A. 2010. Clinical phases and forms of Chagas disease. In: Telleria J, Tibayrenc M. editors. *American trypanosomiasis Chagas disease one hundred years of research*. Amsterdam: Elsevier. p 709-736.
- Rodríguez A, Rioult MG, Ora A, Andrews NW. 1995. A trypanosome-soluble factor induces IP3 formation, intracellular Ca²⁺ mobilization and microfilament rearrangement in host cells. *J Cell Biol*. 129(5):1263-1273.
- Rodriguez A, Samoff E, Rioult MG, Chung A, Andrews NW. 1996. Host cell invasion by trypanosome requires lysosomes and microtubule/kinesin-mediated transport. *J Cell Biol*. 134(2):349-362
- Rodrigues MM, Oliveira AC, Bellio M. 2012. The immune response to *Trypanosoma cruzi* : role of toll-like receptors and perspectives for vaccine development. *J Parasitol Res*. 2012:507874.
- Romagnoli BAA, Picchi GFA, Hiraiwa PM, Borges BS, Alves LR, Goldenberg S. 2018. Improvements in the CRISPR/Cas9 system for high efficiency gene disruption in *Trypanosoma cruzi*. *Acta Trop*. 178:190-195.
- Ruiz AM, Esteva M, Cabeza Meckert P, Laguens RP, Segura EL. 1985. Protective immunity and pathology induced by inoculation of mice with different subcellular fractions of *Trypanosoma cruzi*. *Acta Trop*. 42(4):299-309.
- Sales Junior PA, Molina I, Fonseca Murta SM, Sánchez-Montalvá A, Salvador F, Corrêa-Oliveira R, Carneiro CM. 2017. Experimental and clinical treatment of Chagas disease: a review. *Am J Trop Med Hyg*. 97(5):1289-1303.
- Segura EL, Paulone I, Cerisola J, González Cappa SM. 1976. Experimental Chagas' disease: protective activity in relation with subcellular fractions of the parasite. *J Parasitol*. 62(1):131-133.
- Soares Medeiros LC, South L, Peng D, Bustamante JM, Wang W, Bunkofske M, Perumal N, Sanchez-Valdez F, Tarleton RL. 2017. Rapid, selection-free, high-efficiency genome editing in protozoan parasites using CRISPR-Cas9 ribonucleoproteins. *MBio*. 8(6):e01788-17

- Sosoniuk E, Vallejos G, Kenawy H, Gaboriaud C, Thielens N, Fujita T, Schwaeble W, Ferreira A, Valck C. 2014. *Trypanosoma cruzi* calreticulin inhibits the complement lectin pathway activation by direct interaction with L-ficolin. *Mol Immunol.* 60(1):80-85.
- Steverding D. 2014. The history of Chagas disease. *Parasit Vectors.* 7:317.
- Tambourgi DV, Kipnis TL, da Silva WD, Joiner KA, Sher A, Heath S, Hall BF, Ogden GB. 1993. A partial cDNA clone of trypomastigote decay-accelerating factor (T-DAF), a developmentally regulated complement inhibitor of *Trypanosoma cruzi*, has genetic and functional similarities to the human complement inhibitor DAF. *Infect Immun.* 61(9):3656-3663.
- Thurtle-Schmidt DM, Lo TW. 2018. Molecular biology at the cutting edge: a review on CRISPR/CAS9 gene editing for undergraduates. *Biochem Mol Biol Educ.* 46(2):195-205.
- Trinchieri G, Sher A. 2007. Cooperation of toll-like receptor signals in innate immune defense. *Nat Rev Immunol.* 7(3):179-190.
- Truyens, C, Carlier, Y. 2010. Protective host response to parasite and its limitations. In: Telleria J, Tibayrenc M. editors. *American trypanosomiasis Chagas disease one hundred years of research.* Amsterdam: Elsevier. p 601-642.
- Van Overtvelt L, Vanderheyde N, Verhasselt V, Ismaili J, De Vos L, Goldman M, Willems F, Vrary B. 1999. *Trypanosoma cruzi* infects human dendritic cells and prevents their maturation: inhibition of cytokines, HLA-DR, and costimulatory molecules. *Infect Immun.* 67(8):4033-4040.
- Venturini G, Salvati L, Muolo M, Colasanti M, Gradoni L, Ascenzi P. 2000. Nitric oxide inhibits cruzipain, the major papain-like cysteine proteinase from *Trypanosoma cruzi*. *Biochem Biophys Res Commun.* 270(2):437-441.
- Wheeler R. 2006. Trypanosome flagellum structure. [accessed 2019 May 30].
https://commons.wikimedia.org/wiki/File:Trypanosome_Flagellum_Structure.png
- Wheeler R. 2011. Trypanosomatid morphologies. [accessed 2019 May 31].
https://commons.wikimedia.org/wiki/File:TrypanosomatidMorphologies_PlainSVG.svg
- Woolsey AM, Sunwoo L, Petersen CA, Brachmann SM, Cantley LC, Burleigh BA. 2003. Novel PI 3-kinase-dependent mechanisms of trypanosome invasion and vacuole maturation. *J Cell Sci.* 116(Pt 17):3611-3622.

World Health Organization (WHO). 2019-A. What is Chagas disease; [accessed 2019 Apr 29]. <https://www.who.int/chagas/disease/en/>

World health organization (WHO). 2019-B. Chagas disease (American trypanosomiasis; [accessed 2019 May 29]. [https://www.who.int/news-room/fact-sheets/detail/chagas-disease-\(american-trypanosomiasis\)](https://www.who.int/news-room/fact-sheets/detail/chagas-disease-(american-trypanosomiasis))

Wrightsman RA, Miller MJ, Saborio JL, Manning JE. 1995. Pure paraflagellar rod protein protects mice against *Trypanosoma cruzi* infection. *Infect Immun.* 63(1):122-125.